Doctoral Dissertation

Development of Efficient Fabrication Processes for Nanocellulose Films and Their Applications via Electrophoretic Deposition
(ナノセルロースの電気泳動堆積現象を用いた
フィルム調製手法の開発および応用)

Chenyang LI

Jan 2025

Graduate School of Engineering,
Osaka University

Contents

General Introduction

With growing concern about environmental issues caused by the overexploitation of fossil resources, the demand for bio-based materials to replace conventional petroleum-derived products is steadily growing. Cellulose, the Earth's most abundant renewable biopolymer, shows significant potential due to its primary role as a structural component in plant cell walls.[1,2]

From a top-down perspective, cellulose fibers can be extracted from wood and then broken down into fibrils with progressively smaller diameters (spanning a range from approximately 20–30 μm down to about 2–4 nm) which are ultimately composed of ordered linear cellulose molecular chains (**Figure 1**).[3-8] The recent advancements in nanotechnology have sparked significant interest in exploring cellulose at the nanoscale. Nanocelluloses are characterized as fibers with widths less than 100 nm. Cellulose nanofibers (CNFs), as one group of the fine nanocelluloses, have average lengths exceeding 500 nm and uniform widths of approximately 3 nm.[9]

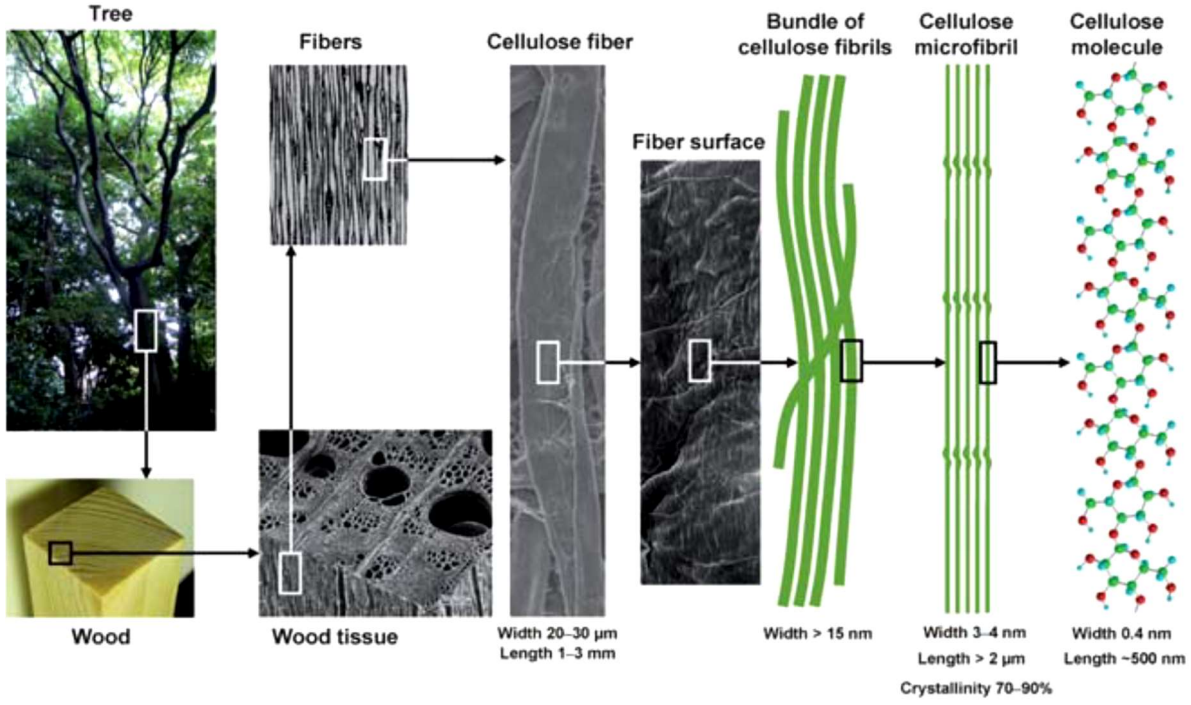

Figure 1. The hierarchical structure of wood biomass and the properties of cellulose microfibrils.[3] Copyright 2011 The Royal Society of Chemistry.

CNFs are typically obtained by mechanical nanofabrication processes[10,11] or chemical pre-treatment[12-16]. Nevertheless, achieving effective dispersion of hydrophilic CNFs within hydrophobic

matrix polymers continues to present a considerable challenge, particularly at the level of individual nanofibrils. Achieving a high degree of dispersion is critical for maximizing the nanocomposite effects while keeping the addition levels as low as possible to ensure material efficiency and cost-effectiveness. The numerous hydroxyl groups on the surface of CNFs introduce further complexities, as they contribute to its strong hydrophilicity.[17] To address these issues, it is essential to establish efficient surface hydrophobization procedures. These procedures should not only be simple and environmentally friendly but also effectively enhance the dispersion of CNFs in hydrophobic matrices. Furthermore, such hydrophobization processes would also improve the moisture and water resistance of the resulting composites, making them more suitable for applications in diverse and demanding environments.

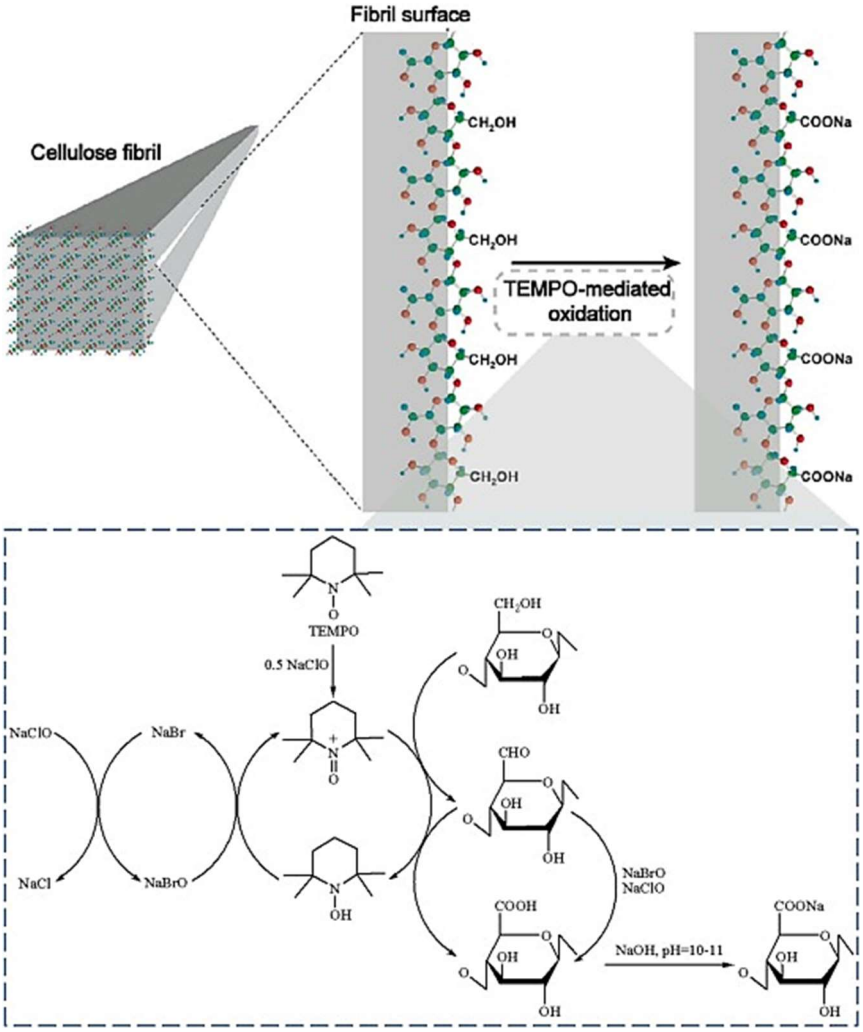

Figure 2. The C6 primary hydroxyl groups of cellulose can be regioselectively oxidized to C6 carboxylate groups through TEMPO/NaBr/NaClO oxidation in aqueous solution, under a pH range of 10 to 11.[30] Copyright 2023 Elsevier.

Numerous surface hydrophobization methods have been explored, including silylation, esterification, and grafting.[18-21] Among these, TEMPO-mediated oxidation has emerged as one of the most commonly employed and straightforward treatments.[3,22-25] TEMPO (2,2,6,6-tetramethylpiperidine-1-oxyl radical) is a stable nitroxyl radical that is commercially available and water-soluble. It facilitates the efficient and selective oxidation of alcoholic hydroxyl groups to aldehydes, ketones, and carboxylic acids under mild conditions. The application of the TEMPO/NaBr/NaClO oxidation system, set at pH 10 and room temperature, to native cellulose with the cellulose I crystal structure results in the oxidation of the C6 primary hydroxyl groups to C6 carboxylate groups **(Figure 2)**.[3, 26] After slight mechanical treatments, TEMPO-oxidized cellulose nanofibers (TOCNs) of 3-4 nm width can be obtained.[22, 23]

TOCNs exhibit excellent dispersibility in water. TOCNs can be dispersed in water as isolated nanofibrils. This is due to the carboxylate groups on the surface, which generate pH-dependent electric double layer repulsion in dispersions and enhance compatibility within the bulk phase.[3,22-25] The carboxylate groups on TOCNs also provide places for further modification. The counterions of the carboxylate groups can be easily converted to various ions via ion-exchange in water.[27-29]

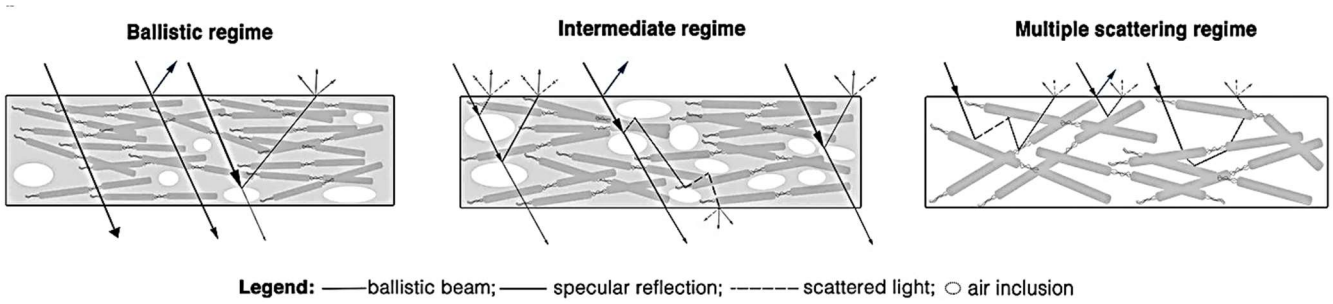

Figure 3. An illustration of various scattering regimes in cellulose-based materials is presented, where the transition between regimes is marked by an increase in the number of air inclusions, leading to enhanced scattering.[37] Copyright 2020 Wiley.

Figure 4. Digital photograph (left) and AFM image (right) of transparent TOCN film.[38] Copyright 2008 American Chemical Society.

The resulting TOCN films, often referred to as "nanopaper," [31, 32] can be prepared from the aqueous TOCN dispersions. In theory, paper produced from cellulose should be optically transparent, as cellulose itself is colorless. In reality, most types of paper, including copy paper, appear opaque. This phenomenon can be attributed to the porous structure of paper, which causes light scattering at the fiber/air interface due to the refractive index mismatch between cellulose (1.5) and air (1.0) (**Figure 3**). [33, 34] To enhance optical transmission in paper, the air present in its porous structure must be minimized as much as possible.[6] Using exceptionally fine fibers, the resulting TOCN film has outstanding optical transparency with low haze (**Figure 4**).[32, 36] This result occurs because the individual fine nanofibers are twisted and physically entangled, creating a high-density network, as shown in **Figure 3 left**. This structure eliminates cavities, thereby preventing light scattering within the sheet.

Other than its unique optical properties, The TOCN film exhibits outstanding flexibility, high tensile strength, and exceptional gas barrier properties under dry conditions.[38-44] The TOCN film also has high heat resistance and can withstand continuous heating up to 150 °C. In addition, its CTE (coefficient of linear thermal expansion) is much lower than that of plastics, measuring 8–10 ppm/K.[45] Besides, the TOCNF film exhibits excellent solvent resistance, maintaining notable stability even after being immersed in various organic solvents for a day.[46] These distinctive properties make TOCN film a promising candidate for sustainable flexible electronics like paper transistors, paper solar cells, paper memories, and so on (**Figure 5**).[47-53]

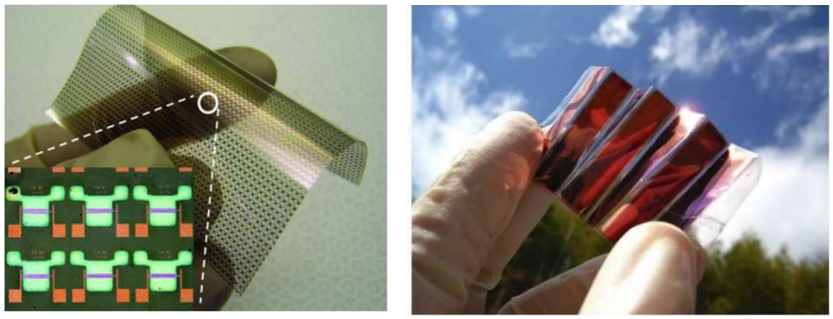

Figure 5. Left: Nanopaper-based transistors.[50] Copyright 2013 Wiley; Right: Nanopaper-based solar cells.[51] Copyright 2015 2025 Springer.

Despite these promising applications, the production and integration of TOCNs into advanced electronics presents several challenges. These challenges include the high energy and time requirements for dehydration and film-making processes.[54,55] Once prepared from wood, the aqueous

TOCN dispersions contain a considerable amount of water. In order to lower transportation and storage expenses, it is necessary to remove large quantities of water from the TOCN dispersions. To produce TOCN films, a slow process such as evaporation or filtration is required. Therefore, developing efficient dehydration methods and preserving key film properties like transparency, and mechanical properties is of great importance.

Moreover, as the growth and industrialization of various sectors have improved people's living standards through the invention of electronic devices, electronic waste has become a significant part of global solid waste management. As a major component of solid waste, E-waste contains numerous hazardous materials, including halogenated compounds and other toxic materials, which adversely impact plants, microbes, and humans.[56-58]

Figure 6. Environmental life cycle assessment of E-waste management.[59] Copyright 2023 Elsevier.

In addition to recycling, finding efficient methods to extend the lifespan of electronics is equally crucial for effective e-waste management (**Figure 6**). By improving the durability and longevity of electronic devices, this work can significantly reduce the amount of waste generated, thereby lessening the environmental impact and promoting sustainability. This approach not only conserves resources but also alleviates the pressure on disposal systems, making it a vital aspect of modern waste management strategies. Therefore, in addition to investigating various applications of sustainable materials for electronics, finding new approaches to protect and extend the life of electronic devices by using sustainable materials like TOCNs is also of great importance.

Purpose and Outline of This Thesis

The primary goal of this thesis is to develop efficient fabrication techniques for nanocellulose films and investigate their potential applications in electronic protection. Specifically, the research focuses on three critical aspects:

Development of Efficient Dehydration Methods: Investigating electrodeposition as an innovative technique for dehydrating TOCN dispersions and forming concentrated hydrogels.

Optimization of Drying Processes: Examining the drying behavior of TOCN films under controlled humidity conditions to reduce fabrication time while maintaining optical clarity.

Application in Electronic Devices: Evaluating the use of ion-exchanged TOCN films as sustainable sealing materials for copper electrodes, aimed at preventing short-circuit failure in electronic devices.

The following sections provide an overview of the key themes addressed in each chapter of the thesis, highlighting the significance of the research contributions to the field of nanomaterials and electronics.

Chapter 1. Electrodeposition of cellulose nanofibers as an efficient dehydration method

One of the fundamental challenges in nanocellulose film fabrication lies in the dehydration of CNF dispersions. The pronounced hydrophilicity and large specific surface area of CNFs result in significant energy and time requirements during conventional drying processes. Various dehydration methods have been proposed, including evaporation, filtration, and centrifugation, but these methods often struggle to achieve efficiency and scalability.

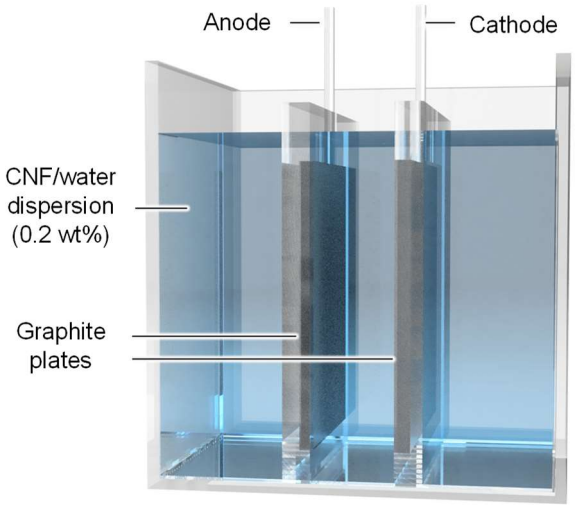

Figure 7. Overview of the electrodeposition system.

This chapter investigates electrodeposition as a novel method for dehydrating CNF dispersions. In this process, negatively charged TOCNs are deposited onto an anode under the influence of a direct current (DC) voltage, resulting in the formation of concentrated hydrogels. This approach not only

enhances dehydration efficiency but also enables structural control of the resulting hydrogels. Furthermore, this chapter explores the preparation of transparent nanopaper from the concentrated CNF hydrogels, demonstrating the potential of electrodeposition as a scalable and efficient fabrication method for nanocellulose-based materials.

Chapter 2. High-Speed Fabrication of Clear Transparent Cellulose Nanopaper by Applying Humidity-Controlled Multi-Stage Drying Method

Transparent nanopaper, a renewable and optically clear material derived from nanocellulose, holds significant promise for applications to flexible electronics, displays, and sensors. However, conventional drying methods, such as evaporation, are time-intensive and limit the scalability of nanopaper production. This chapter delves into the drying behavior of nanocellulose dispersions, emphasizing the role of environmental factors such as relative humidity (RH) and temperature.

Through systematic experimentation, the research demonstrates that RH exerts a more pronounced effect on drying time and haze compared to temperature. Based on these findings, a humidity-controlled multi-stage drying method is proposed to accelerate the fabrication process without compromising the optical and mechanical properties of the nanopaper. The proposed method represents a significant advancement in the high-speed production of transparent nanocellulose films, paving the way for their broader application in electronic devices.

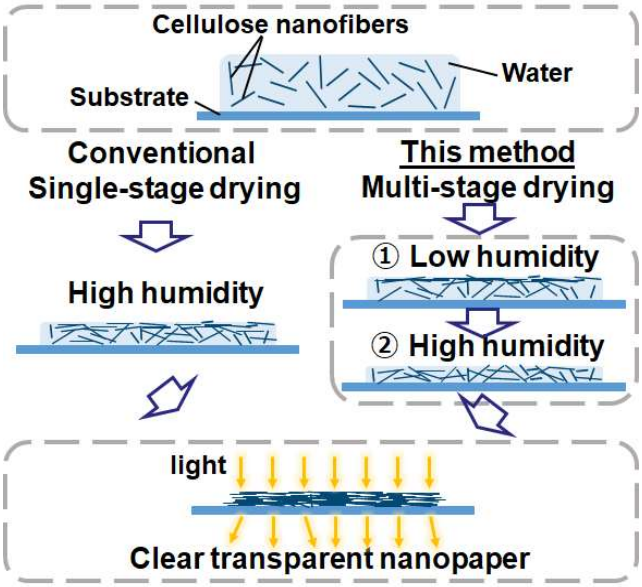

Figure 8. Schematic of a new humidity-regularized multi-stage drying

Chapter 3. Li counterion-exchanged TEMPO-oxidized cellulose nanofibers as a copper electrode seal for short-circuit failure inhibition

Electronic devices are highly susceptible to short-circuit failure caused by water or moisture ingress. Traditionally, epoxy resins and other synthetic materials have been used to seal electrodes and protect against moisture. However, the shift towards sustainable materials is crucial for reducing the environmental impact of electronic manufacturing. This chapter explores the use of ion-exchanged TOCN films as sealing materials for copper electrodes, aiming to prevent water-induced short-circuit failure.

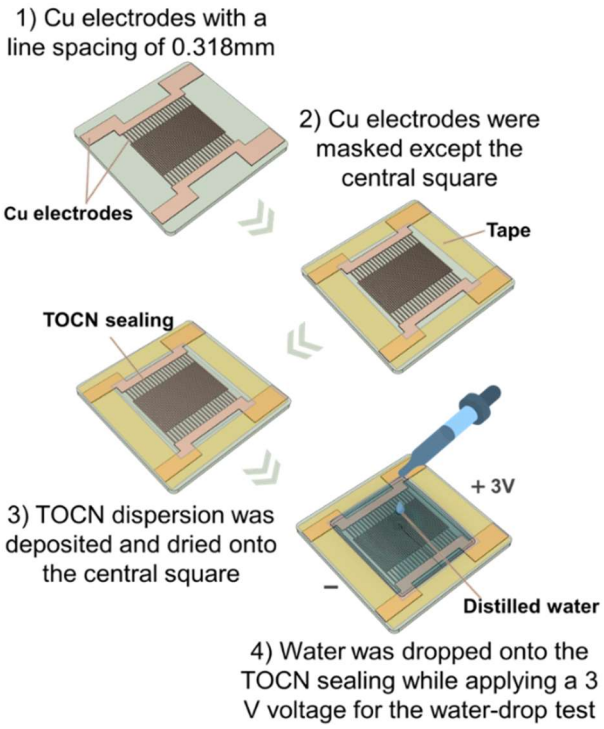

Figure 9. Schematic of TOCN sealing on copper electrode and water-drop test

The research evaluates five types of ion-exchanged TOCNs, examining their performance as moisture barriers and their flame resistance. The findings demonstrate that TOCN films not only effectively inhibit short-circuit failure but also exhibit excellent flame resistance, making them a viable alternative to conventional sealing materials. By integrating sustainable nanomaterials into electronic devices, this chapter highlights the potential for eco-friendly and high-performance electronics.

This thesis makes several important contributions to the fields of nanomaterials science and electronic engineering. First, it introduces electrodeposition as an efficient and scalable method for dehydrating CNF dispersions, addressing a key bottleneck in the fabrication of nanocellulose films. Second, it develops a novel humidity-controlled drying process that significantly reduces the production time of transparent nanopaper while preserving its desirable properties. Finally, it demonstrates the feasibility of using TOCN films as sustainable sealing materials for electronic devices, offering a green alternative to conventional synthetic materials.

In conclusion, this thesis lays the groundwork for developing efficient fabrication techniques for nanocellulose films and their application in advanced electronic protection. By bridging the gap between fundamental research and practical implementation, it contributes to the ongoing transition toward a sustainable and eco-friendly future.

References

1. Li, T.; Chen, C.; Brozena, A. H.; Zhu, J. Y.; Xu, L.; Driemeier, C.; Dai, J.; Rojas, O. J.; Isogai, A.; Wågberg, L.; Hu, L. Developing Fibrillated Cellulose as a Sustainable Technological Material. *Nature* **2021**, *590* (7844), 47–56.
2. Moon, R. J.; Martini, A.; Nairn, J.; Simonsen, J.; Youngblood, J. Cellulose Nanomaterials Review: Structure, Properties and Nanocomposites. *Chem. Soc. Rev.* **2011**, *40* (7), 3941–3994.
3. Isogai, A.; Saito, T.; Fukuzumi, H. TEMPO-Oxidized Cellulose Nanofibers. *Nanoscale* **2011**, *3* (1), 71–85.
4. Ling, S.; Chen, W.; Fan, Y.; Zheng, K.; Jin, K.; Yu, H.; Buehler, M. J.; Kaplan, D. L. Biopolymer Nanofibrils: Structure, Modeling, Preparation, and Applications. *Prog. Polym. Sci.* **2018**, *85*, 1–56.
5. Zhu, H.; Zhu, S.; Jia, Z.; Parvinian, S.; Li, Y.; Vaaland, O.; Hu, L.; Li, T. Anomalous Scaling Law of Strength and Toughness of Cellulose Nanopaper. *Proc. Natl. Acad. Sci. U. S. A.* **2015**, *112* (29), 8971–8976.
6. Zhu, H.; Luo, W.; Ciesielski, P. N.; Fang, Z.; Zhu, J. Y.; Henriksson, G.; Himmel, M. E.; Hu, L. Wood-Derived Materials for Green Electronics, Biological Devices, and Energy Applications. *Chem. Rev.* **2016**, *116* (16), 9305–9374.
7. Wang, Q. Q.; Zhu, J. Y.; Gleisner, R.; Kuster, T. A.; Baxa, U.; McNeil, S. E. Morphological Development of Cellulose Fibrils of a Bleached Eucalyptus Pulp by Mechanical Fibrillation. *Cellulose* **2012**, *19* (5), 1631–1643.
8. Henn, A. R.; Fraundorf, P. B. A Quantitative Measure of the Degree of Fibrillation of Short Reinforcing Fibres. *J. Mater. Sci.* **1990**, *25* (8), 3659–3663.
9. Isogai, A. Emerging Nanocellulose Technologies: Recent Developments. *Adv. Mater.* **2021**, *33* (28), 1–10.
10. Abe, K.; Iwamoto, S.; Yano, H. Obtaining Cellulose Nanofibers with a Uniform Width of 15 nm from Wood. *Biomacromolecules* **2007**, *8* (10), 3276–3278.
11. Kondo, T.; Kose, R.; Naito, H.; Kasai, W. Aqueous Counter Collision Using Paired Water Jets as a Novel Means of Preparing Bio-Nanofibers. *Carbohydr. Polym.* **2014**, *112*, 284–290.
12. Pääkkö, M.; Ankerfors, M.; Kosonen, H.; Nykänen, A.; Ahola, S.; Österberg, M.;

Ruokolainen, J.; Laine, J.; Larsson, P. T.; Ikkala, O.; Lindström, T. Enzymatic Hydrolysis Combined with Mechanical Shearing and High-Pressure Homogenization for Nanoscale Cellulose Fibrils and Strong Gels. *Biomacromolecules* **2007**, *8* (6), 1934–1941.

13. Henriksson, M.; Henriksson, G.; Berglund, L. A.; Lindström, T. An Environmentally Friendly Method for Enzyme-Assisted Preparation of Microfibrillated Cellulose (MFC) Nanofibers. *Eur. Polym. J.* **2007**, *43* (8), 3434–3441.

14. Bhatnagar, A.; Sain, M. Processing of Cellulose Nanofiber-Reinforced Composites. *J. Reinf. Plast. Compos.* **2005**, *24* (12), 1259–1268.

15. Wang, B.; Sain, M. Dispersion of Soybean Stock-Based Nanofiber in a Plastic Matrix. *Polym. Int.* **2007**, *56* (4), 538–546.

16. Wang, B.; Sain, M. Isolation of Nanofibers from Soybean Source and Their Reinforcing Capability on Synthetic Polymers. *Compos. Sci. Technol.* **2007**, *67* (11–12), 2521–2527.

17. Shimizu, M.; Saito, T.; Isogai, A. Bulky Quaternary Alkylammonium Counterions Enhance the Nanodispersibility of 2,2,6,6-Tetramethylpiperidine-1-oxyl-Oxidized Cellulose in Diverse Solvents. *Biomacromolecules* **2014**, *15* (5), 1904–1909.

18. Habibi, Y.; Lucia, L. A.; Rojas, O. J. Cellulose Nanocrystals: Chemistry, Self-Assembly, and Applications. *Chem. Rev.* **2010**, *110*, 3479–3500.

19. Siro, I.; Plackett, D. Microfibrillated Cellulose and New Nanocomposite Materials: A Review. *Cellulose* **2010**, *17*, 459–494.

20. Eichhorn, S. J.; Dufresne, A.; Aranguren, M.; Marcovich, N. E.; Capadona, J. R.; Rowan, S. J.; Weder, C.; Thielemans, W.; Roman, M.; Renneckar, S.; Gindl, W.; Veigel, S.; Keckes, J.; Yano, H.; Abe, K.; Nogi, M.; Nakagaito, A. N.; Mangalam, A.; Simonsen, J.; Benight, A. S.; Bismarck, A.; Berglund, L. A.; Peijs, T. Review: Current International Research into Cellulose Nanofibres and Nanocomposites. *J. Mater. Sci.* **2010**, *45*, 1–33.

21. Klemm, D.; Kramer, F.; Moritz, S.; Lindstrom, T.; Ankerfors, M.; Gray, D.; Dorris, A. Nanocelluloses: A New Family of Nature-Based Materials. *Angew. Chem., Int. Ed.* **2011**, *50*, 5438–5466.

22. Saito, T., Nishiyama, Y., Putaux, J.-L., Vignon, M. & Isogai, A. Homogeneous Suspensions of Individualized Microfibrils from TEMPO-Catalyzed Oxidation of Native Cellulose. *Biomacromolecules* **2006**, *7*, 1687–1691.

23. Saito, T.; Kimura, S.; Nishiyama, Y.; Isogai, A. Cellulose Nanofibers Prepared by TEMPO-Mediated Oxidation of Native Cellulose. *Biomacromolecules* **2007**, *8* (8), 2485–2491.

24. Olszewska, A.; Eronen, P.; Johansson, L.-S.; Malho, J.-M.; Ankerfors, M.; Lindström, T.; Ruokolainen, J.; Laine, J.; Österberg, M. *Cellulose* **2011**, *18*, 1213.

25. Azzam, F.; Moreau, C.; Cousin, F.; Menelle, A.; Bizot, H.; Cathala, B. *Langmuir* **2014**, *30*, 8091–8100.

26. Isogai, T.; Saito, T.; Isogai, A. TEMPO Electromediated Oxidation of Some Polysaccharides Including Regenerated Cellulose Fiber. *Biomacromolecules* **2010**, *11* (6), 1593–1599.

27. Benítez, A. J.; Walther, A. Counterion Size and Nature Control Structural and Mechanical Response in Cellulose Nanofibril Nanopapers. *Biomacromolecules* **2017**, *18* (5), 1642–1653.

28. Shimizu, M.; Saito, T.; Fukuzumi, H.; Isogai, A. *Biomacromolecules* **2014**, *15*, 4320−4325.

29. Shimizu, M.; Kusumi, R.; Saito, T.; Isogai, A. Thermal and Electrical Properties of Nanocellulose Films with Different Interfibrillar Structures of Alkyl Ammonium Carboxylates. *Cellulose* **2019**, *26* (3), 1657–1665.

30. Tang, Z.; Lin, X.; Yu, M.; Mondal, A. K.; Wu, H. Recent Advances in TEMPO-Oxidized Cellulose Nanofibers: Oxidation Mechanism, Characterization, Properties, and Applications. *Int. J. Biol. Macromol.* **2024**, *259*, 129081.

31. Nogi, M.; Iwamoto, S.; Nakagaito, A. N.; Yano, H. Optically Transparent Nanofiber Paper. *Adv. Mater.* **2009**, *21*, 1595–1598.

32. Fukuzumi, H.; Saito, T.; Iwata, T.; Kumamoto, Y.; Isogai, A. Transparent and High Gas Barrier Films of Cellulose Nanofibers Prepared by TEMPO-Mediated Oxidation. *Biomacromolecules* **2009**, *10*, 162–165.

33. Hubbe, M. A.; Pawlak, J. J.; Koukoulas, A. A. Paper's Appearance: A Review. *BioResources* **2008**, *3*, 627–665.

34. Fang, Z.; Zhu, H.; Preston, C.; Han, X.; Li, Y.; Lee, S.; Chai, X.; Chen, G.; Hu, L. Highly Transparent and Writable Wood All-Cellulose Hybrid Nanostructured Paper. *J. Mater. Chem. C* **2013**, *1* (39), 6191–6197.

35. Henriksson, M.; Berglund, L. A.; Isaksson, P.; Lindström, T.; Nishino, T. Cellulose Nanopaper Structures of High Toughness. *Biomacromolecules* **2008**, *9*, 1579–1585.

36. Nogi, M.; Iwamoto, S.; Nakagaito, A. N.; Yano, H. Optically Transparent Nanofiber Paper. *Adv. Mater.* **2009**, *21*, 1595–1598.

37. Jacucci, G.; Schertel, L.; Zhang, Y.; Yang, H.; Vignolini, S. Light Management with Natural Materials: From Whiteness to Transparency. *Adv. Mater.* **2021**, *33* (28), 2101210.

38. Fukuzumi, H.; Saito, T.; Iwata, T.; Kumamoto, Y.; Isogai, A. Transparent and High Gas Barrier Films of Cellulose Nanofibers Prepared by TEMPO-Mediated Oxidation. *Biomacromolecules* **2009**, *10*, 162–165.

39. Huang, J.; Zhu, H.; Chen, Y.; Preston, C.; Rohrbach, K.; Cumings, J.; Hu, L. Highly Transparent and Flexible Nanopaper Transistors. *ACS Nano* **2013**, *7*, 2106–2113.

40. Hsieh, M.-C.; Kim, C.; Nogi, M.; Suganuma, K. Electrically Conductive Lines on Cellulose Nanopaper for Flexible Electrical Devices. *Nanoscale* **2013**, *5*, 9289.

41. Fujisaki, Y.; Koga, H.; Nakajima, Y.; Nakata, M.; Tsuji, H.; Yamamoto, T.; Kurita, T.; Nogi, M.; Shimidzu, N. Transparent Nanopaper-Based Flexible Organic Thin-Film Transistor Array. *Adv. Funct. Mater.* **2014**, *24*, 1657–1663.

42. Sehaqui, H.; Liu, A.; Zhou, Q.; Berglund, L. A. Fast Preparation Procedure for Large, Flat Cellulose and Cellulose/Inorganic Nanopaper Structures. *Biomacromolecules* **2010**, *11* (9), 2195–2198.

43. Nogi, M.; Kim, C.; Sugahara, T.; Inui, T.; Takahashi, T.; Suganuma, K. High Thermal Stability of Optical Transparency in Cellulose Nanofiber Paper. *Appl. Phys. Lett.* **2013**, *102* (18).

44. Henriksson, M.; Berglund, L. A.; Isaksson, P.; Lindström, T.; Nishino, T. Cellulose Nanopaper Structures of High Toughness. *Biomacromolecules* **2008**, *9* (6), 1579–1585.

45. Yagyu, H.; Saito, T.; Isogai, A.; Koga, H.; Nogi, M. Chemical Modification of Cellulose Nanofibers for the Production of Highly Thermal Resistant and Optically Transparent Nanopaper for Paper Devices. *ACS Appl. Mater. Interfaces* **2015**, *7* (39), 22012–22017.

46. Kuang, Y.; Chen, G.; Ming, S.; Wu, Z.; Fang, Z. Solvent Resistance of 2,2,6,6-Tetramethylpiperidine-1-oxyl (TEMPO) Treated Cellulose Nanofiber Film for Flexible Electronics. *Cellulose* **2016**, *23*, 1979–1987.

47. Eichhorn, S. J.; Dufresne, A.; Aranguren, M.; Marcovich, N. E.; Capadona, J. R.; Rowan, S. J.; Weder, C.; Thielemans, W.; Roman, M.; Renneckar, S.; Gindl, W.; Veigel, S.; Keckes, J.; Yano, H.; Abe, K.; Nogi, M.; Nakagaito, A. N.; Mangalam, A.; Simonsen, J.; Benight, A. S.;

Bismarck, A.; Berglund, L. A.; Peijs, T. Review: Current International Research into Cellulose Nanofibres and Nanocomposites. *J. Mater. Sci.* **2010**, *45*, 1–33.

48. Dias, O. A. T.; Konar, S.; Leão, A. L.; Yang, W.; Tjong, J.; Sain, M. Current State of Applications of Nanocellulose in Flexible Energy and Electronic Devices. *Front. Chem.* **2020**, *8* (May).

49. Hsieh, M.-C.; Kim, C.; Nogi, M.; Suganuma, K. Electrically Conductive Lines on Cellulose Nanopaper for Flexible Electrical Devices. *Nanoscale* **2013**, *5*, 9289.

50. Fujisaki, Y.; Koga, H.; Nakajima, Y.; Nakata, M.; Tsuji, H.; Yamamoto, T.; Kurita, T.; Nogi, M.; Shimidzu, N. Transparent Nanopaper-Based Flexible Organic Thin-Film Transistor Array. *Adv. Funct. Mater*. **2014**, *24*, 1657–1663.

51. Nogi, M.; Karakawa, M.; Komoda, N.; Yagyu, H.; Nge, T. T. Transparent Conductive Nanofiber Paper for Foldable Solar Cells. *Sci. Rep.* **2015**, *5*, 17254.

52. Celano, U.; Nagashima, K.; Koga, H.; Nogi, M.; Zhuge, F.; Meng, G.; He, Y.; De Boeck, J.; Jurczak, M.; Vandervorst, W.; Yanagida, T. All-Nanocellulose Nonvolatile Resistive Memory. *NPG Asia Mater.* **2016**, *8*, e310–e310.

53. Inui, T.; Koga, H.; Nogi, M.; Komoda, N.; Suganuma, K. A Miniaturized Flexible Antenna Printed on a High Dielectric Constant Nanopaper Composite. *Adv. Mater.* **2015**, *27*, 1112–1116.

54. Syverud, K.; Stenius, P. Strength and Barrier Properties of MFC Films. *Cellulose* **2009**, *16* (1), 75–85.

55. Aulin, C.; Gällstedt, M.; Lindström, T. Oxygen and Oil Barrier Properties of Microfibrillated Cellulose Films and Coatings. *Cellulose* **2010**, *17* (3), 559–574.

56. Robinson, B. H. E-Waste: An Assessment of Global Production and Environmental Impacts. *Sci. Total Environ.* **2009**, *408*, 183–191.

57. Wong, M. H.; Wu, S. C.; Deng, W. J.; Yu, X. Z.; Luo, Q.; Leung, A. O. W.; Wong, C. S. C.; Luksemburg, W. J.; Wong, A. S. Export of Toxic Chemicals – A Review of the Case of Uncontrolled Electronic-Waste Recycling. *Environ. Pollut.* **2007**, *149*, 131–14

58. Saha, L.; Kumar, V.; Tiwari, J.; Rawat, S.; Singh, J.; Bauddh, K. Electronic Waste and Their Leachates Impact on Human Health and Environment: Global Ecological Threat and Management. *Environ. Technol. Innov.* **2021**, *24*, 102049.

59. He, Y.; Kiehbadroudinezhad, M.; Hosseinzadeh-Bandbafha, H.; Gupta, V. K.; Peng, W.; Lam, S. S.; Aghbashlo, M. Driving Sustainable Circular Economy in Electronics: A Comprehensive Review on Environmental Life Cycle Assessment of E-Waste Recycling. *Environ. Pollut.* **2024**, *342*, 123081.

Chapter 1: Electrodeposition of Cellulose Nanofibers as an Efficient Dehydration Method

1.1 Introduction

Cellulose nanofibers (CNFs) have attracted much attention as sustainable nanomaterials due to their excellent properties, such as mechanical strength, transparency, thermal resistance, high surface area, and biodegradability.[1-3] Various application studies with CNFs, including films, filters, hydrogels, aerogels, electronic substrates, and composites, have been reported.[4-11] CNFs are sustainable functional nanomaterials and are expected to be used as alternatives to petroleum-derived materials. In recent years, industrial production of CNFs has increased, especially in Japan, and CNF production facilities are being expanded for mass production. To achieve mass production and mass use of CNFs, it is important to consider the entire life cycle, including the production process and the transportation and storage costs.

CNFs are typically prepared from wood pulp via aqueous fibrillation.[1-3] CNF/water dispersions have high viscosity even at low concentrations;[12] therefore, after preparation, the dispersions contain a large amount of water for effective fibrillation and homogenization. To reduce the transportation and storage costs, removal of large amounts of water from the CNF/water dispersions is necessary.[13-17] CNFs, which are hydrophilic nanofibers, have a high affinity for water and a high surface area;[1-3] therefore, the removal of water from CNF/water dispersions requires enormous amounts of energy and time. Various approaches have been explored for dehydration of CNF/water dispersions, including filtration, evaporation, osmotic concentration, freeze–thaw cycling, and centrifugation.[16, 17-22] Vacuum filtration is a commonly used technique for dehydration of CNF/water dispersions. However, filtration is very time consuming because independently dispersed CNFs, such as 2,2,6,6-tetramethylpiperidine-1-oxylradical (TEMPO)-oxidized CNFs, form a fine network structure on the filter, preventing dehydration. For example, if a 0.2 wt% CNF/water dispersion was dehydrated by filtration, only 52.5% water was dehydrated after 24 h (**Figure 1-3**). Evaporation such as a cast drying method and using a rotary evaporator can dehydrate faster than filtration with higher energy consumption due to the heat of evaporation. Currently, there are two options: fast dehydration with high energy consumption (e.g., evaporation) or low energy consumption for a long time (e.g., filtration, osmotic dewatering). It is not easy to achieve both high-speed dehydration and high energy efficiency.

Electrodeposition of nanocellulose, including CNFs, has attracted much attention in recent years.[23-27] CNFs dispersed in water are negatively charged.[2] When a DC voltage is applied to a

CNF/water dispersion, the CNFs are deposited on the anode by electrodeposition.[23-27] The deposited CNFs form a hydrogel that is several times more concentrated than the dispersion due to electroosmosis.[27-29] Electrodeposition is a potential efficient dehydration method because it does not require water evaporation, which generates energy losses. However, the dehydration efficiency of electrodeposition for independently dispersed CNF/water dispersions, which are the most difficult to dehydrate, is still unclear. When CNFs are deposited electrophoretically, electrochemical reactions on the anode surface convert the counterions of the CNFs.[24-27] It has also been suggested that there may be inhomogeneous cross-linking between CNFs during hydrogel formation on the anode.[27] Uncontrolled orientations and cross-linking of CNFs limit their use after dehydration.[13, 14] Therefore, the structural and chemical states of CNFs during electrodeposition should be evaluated in detail. In addition, it is necessary to determine reuse efficiency of the concentrated CNF hydrogels after electrodeposition.

Herein, this chapter evaluated the electrodeposition of CNFs as a dehydration method. This chapter focused on the dehydration efficiency and the chemical and structural characteristics of the concentrated CNF hydrogels at the anode. In addition, a process for preparing transparent nanopapers from concentrated CNF hydrogels formed on an anode was investigated.

1.2 Experimental Section

1.2.1 Preparation of CNF/water dispersions

TEMPO-oxidized cellulose pulp (carboxyl content: 1.8 mmol/g) was supplied by DKS Co., Ltd. The 0.5 wt% TEMPO-oxidized cellulose pulp slurry was homogenized using a high-pressure water-jet system (HJP-25008, Sugino Machine Co., Ltd., Japan) equipped with a ball-collision chamber. The slurry was repeatedly passed through a small nozzle (diameter: 0.15 mm) under a pressure of 200 MPa. The resulting dispersion was adjusted to a concentration of 0.2 wt% for subsequent use.

1.2.2. Electrodeposition

Two 10 × 10 × 0.5 cm graphite electrodes were placed in an acrylic cell (with a distance of 3 cm between the electrodes), and the cell was filled with 2 L of a 0.2 wt% CNF/water dispersion. Voltages ranging from 1 to 10 V were applied with a source measurement unit (B2902A, Keysight Technologies, USA). The CNF/water dispersion maintained the ambient temperature (~25 °C)

throughout the entire voltage treatment. The concentration of the formed CNF hydrogel was quantified by drying at 110 °C. Voltages of 2.5, 5, and 10 V were required for 1, 3, and 6 h, respectively, to grow each hydrogel to a thickness of 5 mm. Squares (20 × 20 mm) were collected from the centers of the formed CNF hydrogels and used for structural characterization. Fourier Transform Infrared (FT-IR) spectra of CNF films prepared by drying the CNF hydrogels was obtained with an FT-IR spectrometer (Frontier TN, PerkinElmer Inc., USA). The cross-sections of the CNF hydrogels were observed through a cross-sectional polarized optical microscope (ECLIPSE LV100N POL, Nikon Corp., Japan).

1.2.3 Demonstration of filtration dehydration

500 g of 0.2 wt% CNF/water dispersion, the same as used for electrodeposition, was used. A PTFE membrane filter with a pore size of 0.1 μm and a diameter of 90 mm was used. Filtration was performed by reducing the pressure to 0.04 MPa. The amount of dehydrated water after 1 h and 24 h was measured and the dehydration rate from the initial water amount was calculated.

1.2.4 FE-SEM observations

CNF aerogels were prepared by exchange of the water in the CNF hydrogels with ethanol, followed by supercritical drying (SYGLCP-81, JEOL Ltd., Japan). The osmium-treated cross-sections of the CNF aerogels were examined with field-emission scanning electron microscopy (FE-SEM S-4800, Hitachi, Japan) at 2 kV.

1.2.5 Reusability test

CNF hydrogels prepared with a voltage of 10 V and a deposition time of 1 h were used for the reusability tests. For redispersion, the CNF hydrogels were simply homogenized at 8,000 rpm for 10 min with a homogenizing mixer (MARKII Model 2.5, PRIMIX Corp., Japan) and diluted to 0.2 wt%. For neutralization, a 0.1 M sodium hydroxide solution was added to the redispersed CNF dispersion until the pH of the dispersion reached 7. The original, redispersed, and neutralized CNF/water dispersions were then cast-dried at 10 °C and 90% RH to prepare CNF films (film thicknesses of ~18 μm). The total light transmittances of the CNF/water dispersions and CNF films were measured with a UV–vis-NIR spectrophotometer (UV-3600 Plus, Shimadzu Corp., Japan). The hazes and total transmittances of the CNF films were measured with a haze meter (NDH 8000, Nihon Dempa Kogyo

Co., Ltd., Tokyo, Japan). The surface roughnesses were determined with a laser microscope (VK-X3000, Keyence Corp., Japan).

1.3 Results and Discussion

1.3.1. Dehydration of CNF/water dispersions by electrodeposition

A 0.2 wt% TEMPO-oxidized CNF/water dispersion was used as the dehydrating target. The graphite electrodes were placed 3 cm from each other in a CNF/water dispersion, and DC voltages ranging from 1 to 10 V were applied between the electrodes. The CNF hydrogels formed on the anode were collected, and the CNF concentrations of the hydrogels were measured (**Figure 1-1 a-c**). When 1 V was applied, no CNF hydrogel formed on the anode, and the concentration of the CNF/water dispersion near the anode remained the same as the initial concentration (**Figure 1-1 c**). When 2.5–10 V was applied, CNF hydrogels were formed on the anode (**Figure 1-1 c**), and the CNF concentrations of the CNF hydrogels increased beyond the initial concentration (0.2 wt%). When 10 V was applied between the electrodes, CNF hydrogels with CNF concentrations of ~1.58 wt% were formed on the anode after 1 h, which was approximately 8 times more concentrated than the initial concentration. The concentrations of the deposited CNF hydrogels increased slowly as the electrodeposition time was extended beyond 1 h (**Figure 1-1 c**). During electrodeposition, deposition of the CNFs at the anode and concentration via electroosmosis proceed simultaneously.[24-27] Therefore, even if the electrodeposition time was extended, the overall concentration of the CNF hydrogel did not increase substantially. The CNF concentration after electrodeposition for 1 h at different voltages linearly increased with the rise in the applied voltage (**Figure 1-2**). These results suggested that repeated short-term electrodeposition at high voltage and collection of the deposited CNF hydrogel was more effective than long-term electrodeposition.

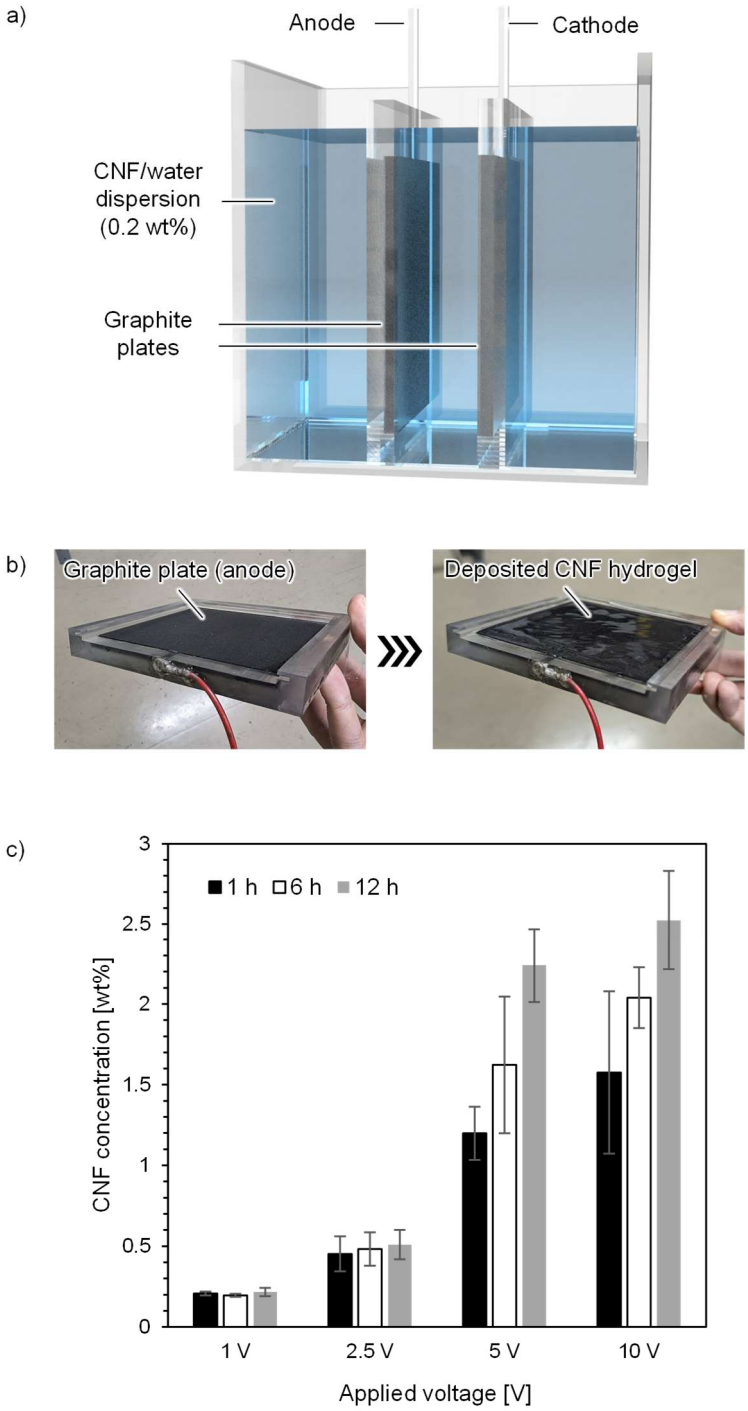

Figure 1-1. a) Overview of the electrodeposition system. **b)** CNF hydrogels were formed on the anode by electrodeposition. **c)** Relationships between the applied voltages, application times and CNF concentrations of CNF hydrogels prepared by electrodeposition.

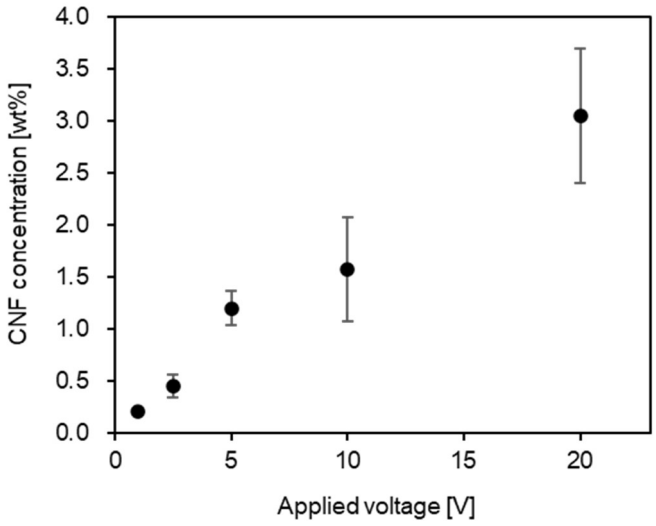

Figure 1-2. CNF concentration after electrodeposition at different voltages for 1 h

1.3.2. Comparison of the dehydration energy efficiencies for evaporation and electrodeposition

The energy consumed in dehydrating 1 g of water was calculated based on the amount of deposited CNFs, the CNF concentration and the energy consumption (**Table 1-1**). As a result, the energy consumption was ~0.0021 [Wh/g] when 10 V was applied for 1 h. The vaporization energy of water (~0.63 [Wh/g], @ 100 °C) was used for comparison.[28] These results suggested that electrodeposition dehydrated the CNF/water dispersions ~300 times more efficiently than evaporation (**Figure 1-4**). When electrodeposition (@ 10 V) was used to dehydrate a 0.2 wt% CNF/water dispersion, ~87% of the water was removed in 1 h with high energy efficiency, making this a promising dehydration method for individually dispersed CNFs such as TEMPO-oxidized CNFs.

Table 1-1. Data used to calculate dehydration efficiency by electrodeposition (@10 V, 1h)

Hydrogel concentration [wt%]	Hydrogel weight [g]	CNF weight [g]	Dehydrated amount [g]	Consumed Energy [Wh]	Energy Consumption [Wh/g]
1.576 ± 0.50	49.92 ± 8.47	0.78 ± 0.24	338.37 ± 120.40	0.64 ± 0.05	0.0021 ± 0.0007

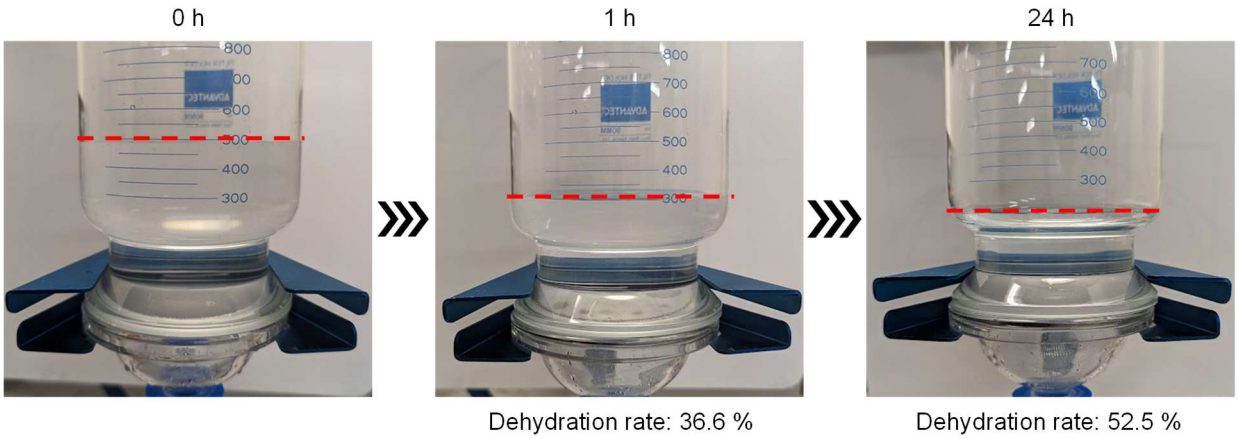

Figure 1-3. Demonstration of filtration dehydration of CNF/water dispersion; it is well known that individually dispersed CNFs, such as TEMPO-oxidized CNFs, require an extremely long time for filtration.

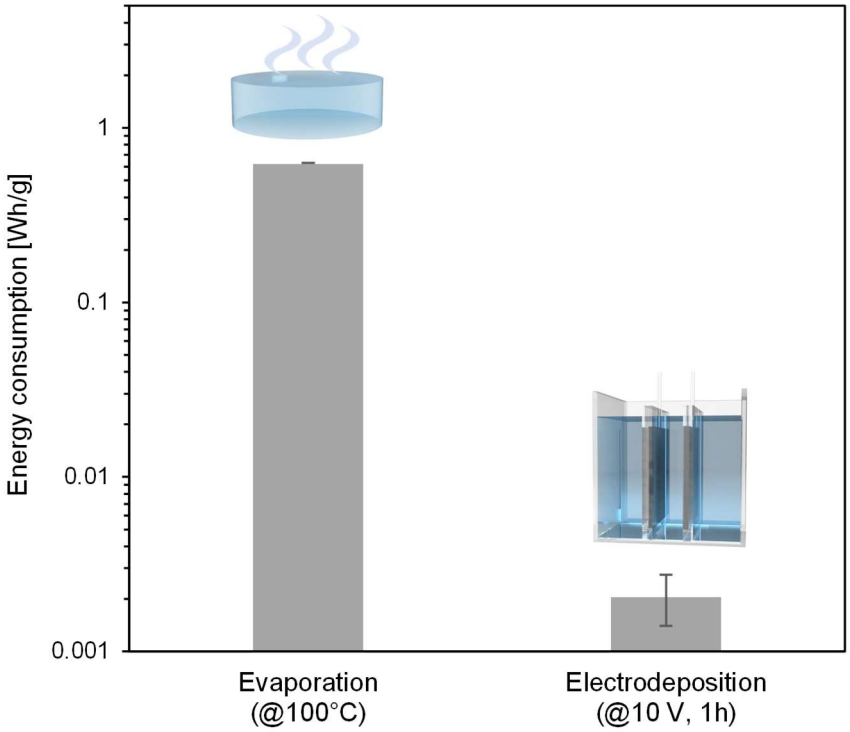

Figure 1-4. Comparison of the dehydration energy consumed by evaporation and electrodeposition

1.3.3. Counterion exchange of CNFs by electrodeposition

During electrodeposition at applied voltages of 2.5 V, 5 V and 10 V, the Na counterions (-COONa) of the CNFs were almost completely replaced with H (-COOH) (**Figure 1-5**).[30, 31] Protonation of the carboxy groups occurred because of the low pH around the anode caused by water electrolysis.[24-27] The initial pH of the CNF/water dispersion were ~6.8. After electrodeposition at 10 V for 1 h, the pH of the dispersion increased to ~10.7. The pH change was caused by water electrolysis and ion-exchange of protons (H^+) with the counter ion of carboxylate groups of CNFs (Na^+). It is thought that the hydroxide ions (OH^-) produced at the cathode became more abundant relative to protons (H^+) by the ion-exchange, resulting in an increase in pH. In the case of electrodeposition at 2.5 V, a peak was observed that appeared to be from the residual sodium carboxylate groups (-COONa). This implied that some Na-type CNFs were not immediately converted to H-type CNFs during electrodeposition in the mild water electrolysis reactions. CNF hydrogels were not formed by electrodeposition at 1 V, and the Na counterions of the CNFs near the anode remained (**Figure 1-5**). It has been reported that CNF hydrogels were formed even at an applied voltage of 1 V when copper was used as the anode.[27] In this study, a graphite electrode was used as the anode, and no hydrogel was formed at an applied voltage of 1 V. With a copper electrode, CNF hydrogel formation was possible because the CNFs were cross-linked and fixed by the copper ions dissolved from the anode.[27] On the other hand, in the case of the graphite anode, electrode dissolution did not occur; therefore, water electrolysis was essential for hydrogel formation.

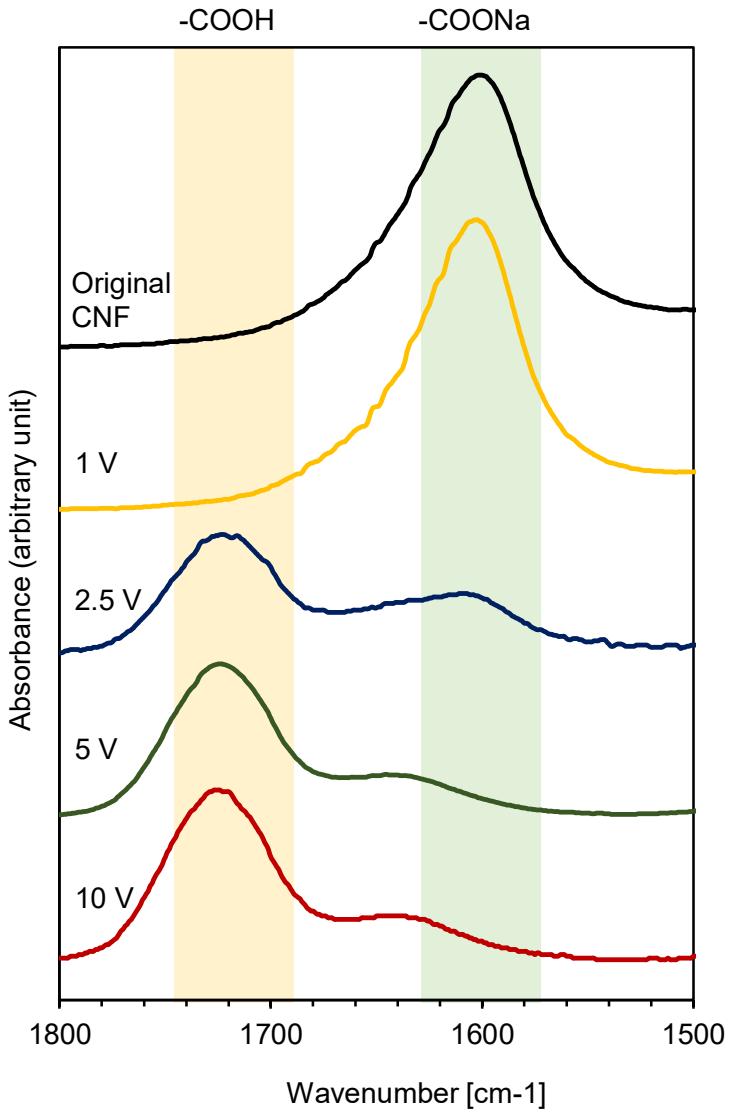

Figure 1-5. FTIR spectra of the deposited CNFs after 1 h with different applied voltages.

1.3.4. Structural effects of electrodeposition on deposited CNF hydrogels

The structural characteristics of the deposited CNF hydrogels were then evaluated. The hydrogel deposited at 2.5 V had a clear appearance with no bubbles and a smooth surface (**Figure 1-6 a, b**). On the other hand, the CNF hydrogels deposited at 5 V and 10 V had translucent appearances containing bubbles, and the gel surfaces were not smooth (**Figure 1-6 c-f**). The bubbles were most likely generated at the anode during the water electrolysis.[24-27] At an applied voltage of 2.5 V, the water electrolysis was milder than those at 5 V and 10 V, suggesting that the oxygen diffused into the water before the bubbles grew, and the bubbles did not grow to visible sizes.[32] Cross-sections of the CNF hydrogels showed that

the interiors of the hydrogels deposited at 2.5 V tended to be uniform and oriented horizontally with respect to the anode surface (**Figure 1-6 b; Figure 1-7**). On the other hand, the internal structures of the hydrogels prepared at 5 V and 10 V were disordered and showed nonuniform tendencies (**Figure 1-6 d, f; Figure 1-7**). There are several possibilities for the changes occurring in the CNF orientations and hierarchical structures with applied voltage. Bubbles in the CNF hydrogels may be one factor; however, there was a report that the out-of-plane CNF orientation was changed by an applied voltage without bubbles.[27] The hierarchical structures of the CNFs in a hydrogel is an important parameter for several applications, such as film preparation,[23, 27] and further investigation of the underlying mechanism is needed.

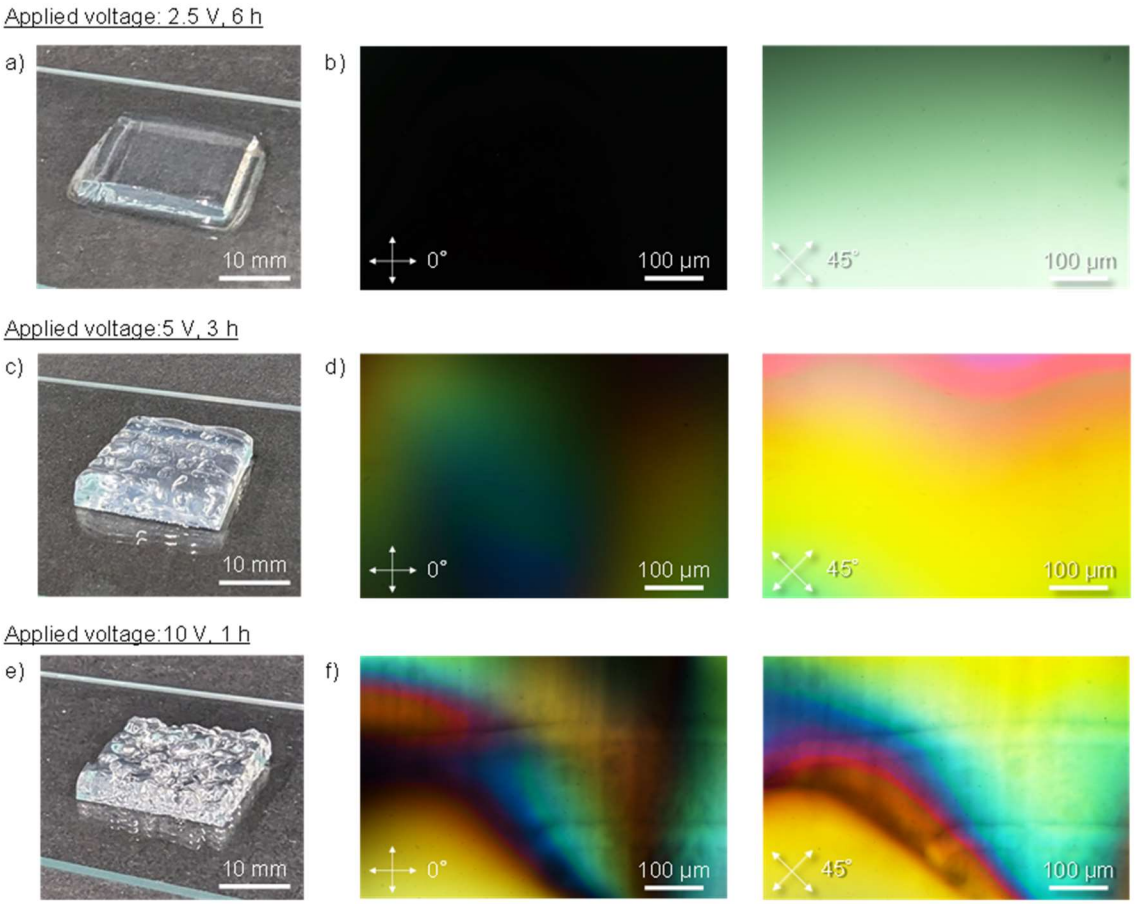

Figure 1-6. CNF hydrogels formed by electrodeposition at applied voltages of **a)**, **b)** 2.5 V, **c)**, **d)** 5 V, and **e)**, **f)** 10 V and cross-sectional polarized optical microscopy images.

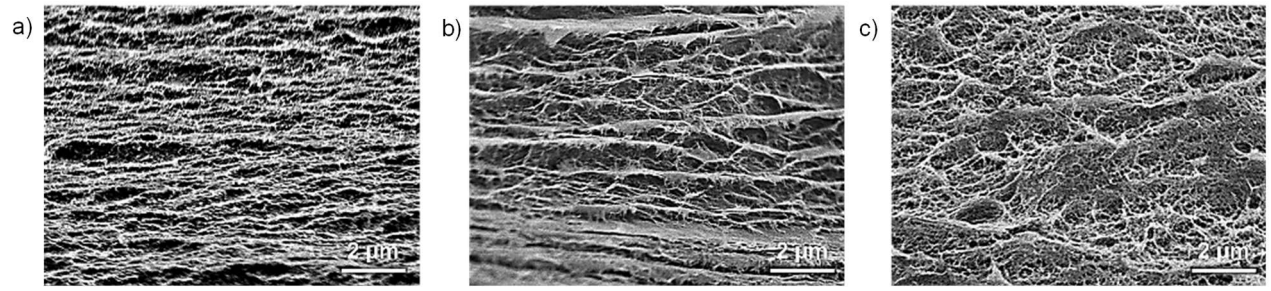

Figure 1-7. Cross-sections of CNF hydrogels prepared by electrodeposition at a) 2.5 V, b) 5 V, and c) 10 V.

1.3.5. Reuse of concentrated CNF hydrogels by electrodeposition

Finally, the reusabilities of concentrated CNF hydrogels were investigated. When a CNF hydrogel was simply diluted and homogenized (**Figure 1-8 a**), light transmittance of the dispersion was maintained at the original level (**Figure 1-8 b**). When large-scale CNF aggregates remained in the dispersion, the light transmittance of the dispersion decreased.[33] This confirmed that after electrodeposition, the CNF hydrogel was redispersed to some extent by dilution and homogenization. CNF films were then prepared by drying the redispersed dispersion (**Figure 1-9 a**). The appearance of the prepared CNF film was clearly transparent (**Figure 1-10**). The total transmittance of the dried CNF film prepared by drying of the redispersed CNF/water dispersion did not decrease (**Figure 1-11**). However, the haze of the film increased, and the film became slightly translucent (**Figure 1-9 b**). The surface roughness of the CNF film was also higher than that of the original dispersion (**Figure 1-9 c**). The carboxyl groups on the surface of the deposited CNF hydrogels were protonated, and the CNFs formed a network structure.[34] Therefore, simple dilution and homogenization of the CNF hydrogels may have left small CNF aggregates, resulting in the increased haze.[13, 14] Neutralization was used to disintegrate the CNF aggregates. A 0.1 M sodium hydroxide solution was added to the CNF dispersion until the pH of the dispersion reached 7. As a result, the haze and surface roughness levels of the dried CNF films were returned to those of the original film (**Figure 1-9 b, c**). These results confirmed that the concentrated CNF hydrogel obtained by electrodeposition could be redispersed via a simple neutralization process.

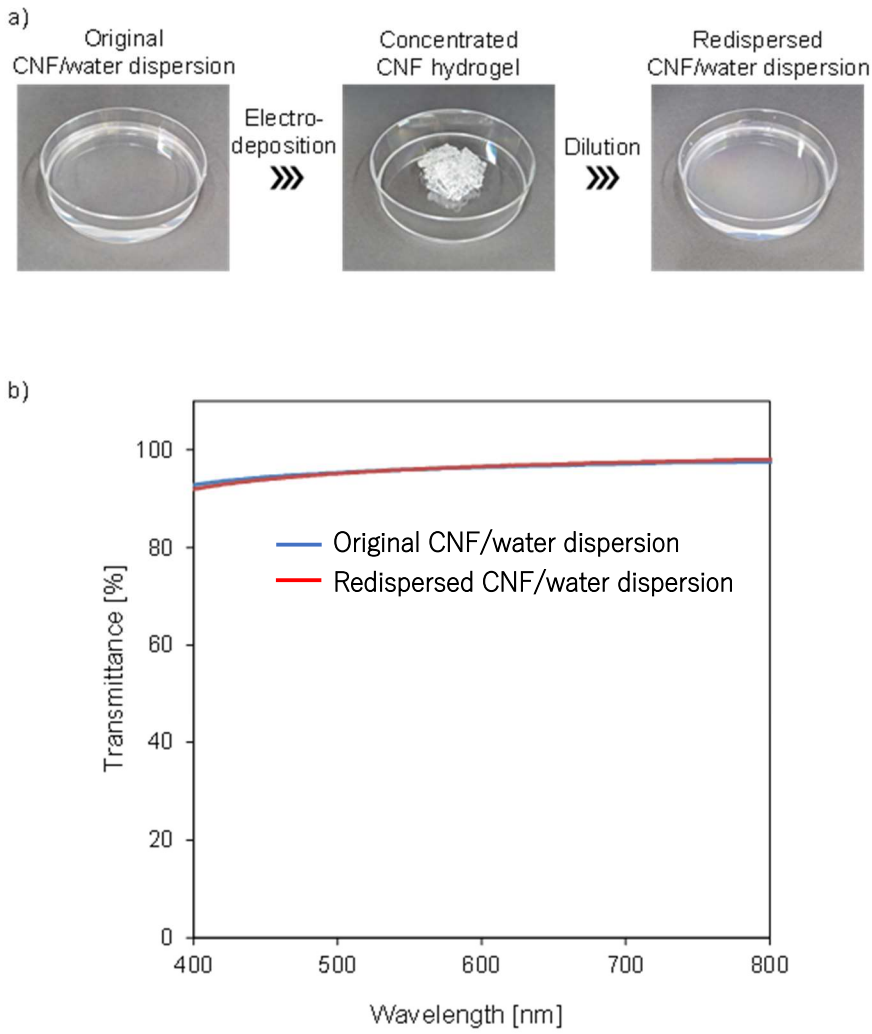

Figure 1-8. **a)** Concentrated CNF hydrogels formed by electrodeposition were redispersed by a simple dilution and agitation process. **b)** The redispersed CNF/water dispersion exhibited almost the same transparency as the original dispersion.

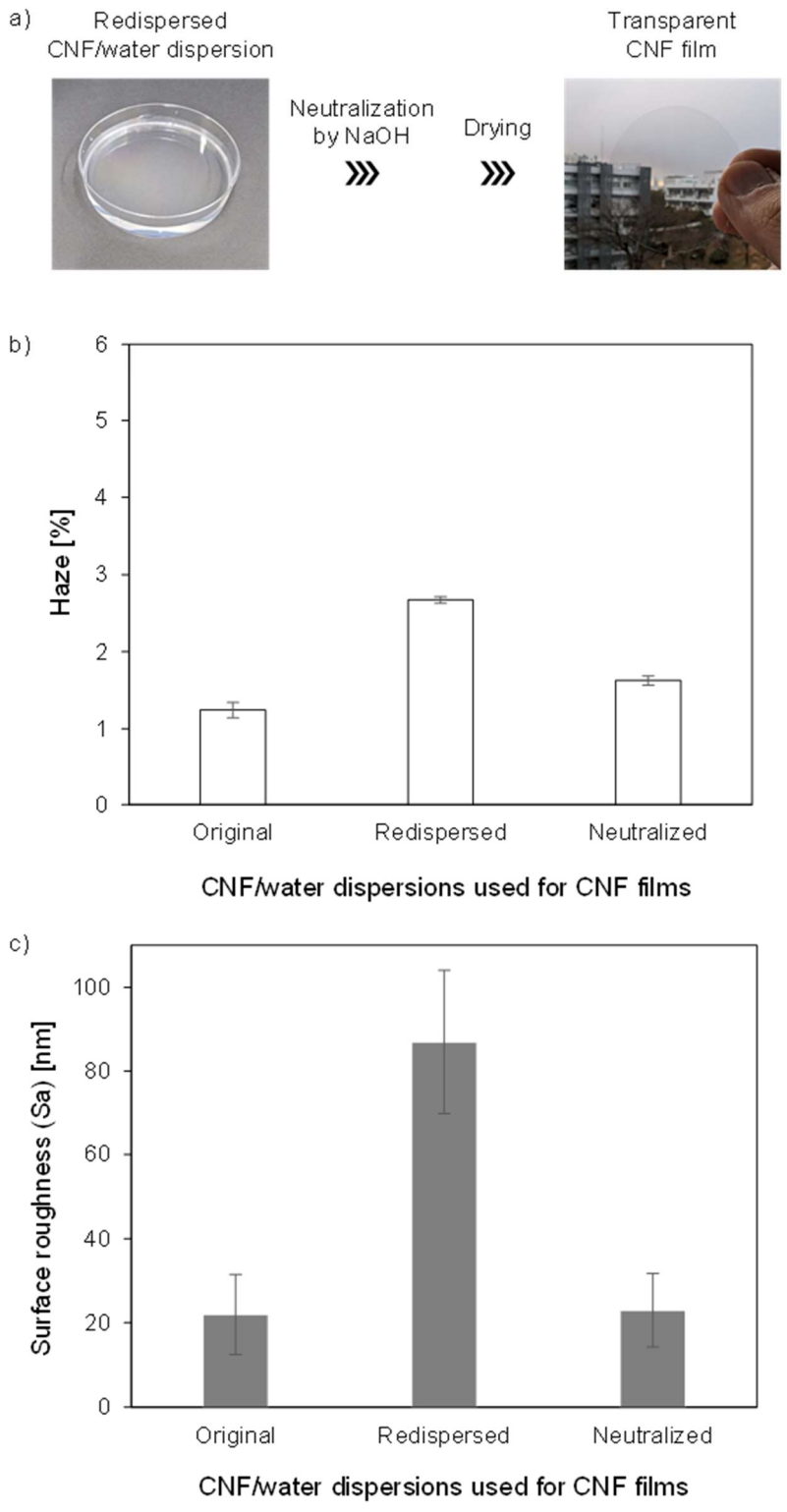

Figure 1-9. a) CNF film preparation from a redispersed CNF/water dispersion. **b)** Haze and c) surface roughness of the CNF films prepared from the original, redispersed, and neutralized CNF/water dispersions.

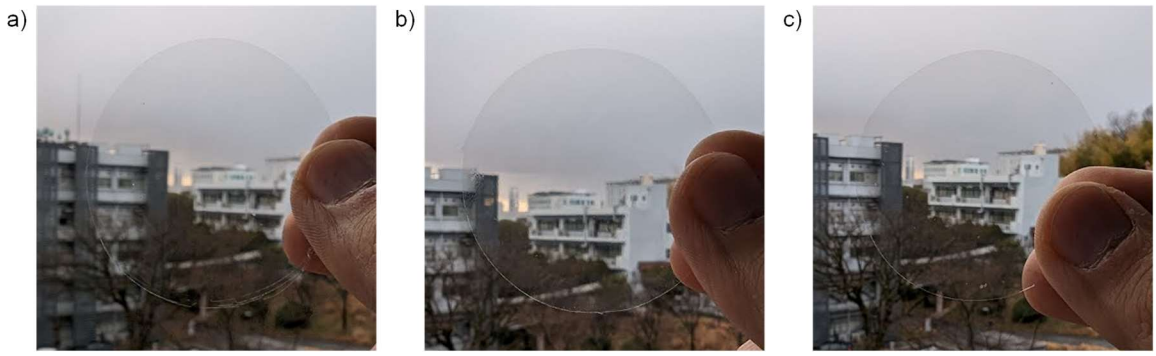

Figure 1-10. CNF films prepared from a) original, b) redispersed and c) neutralized CNF/water dispersions.

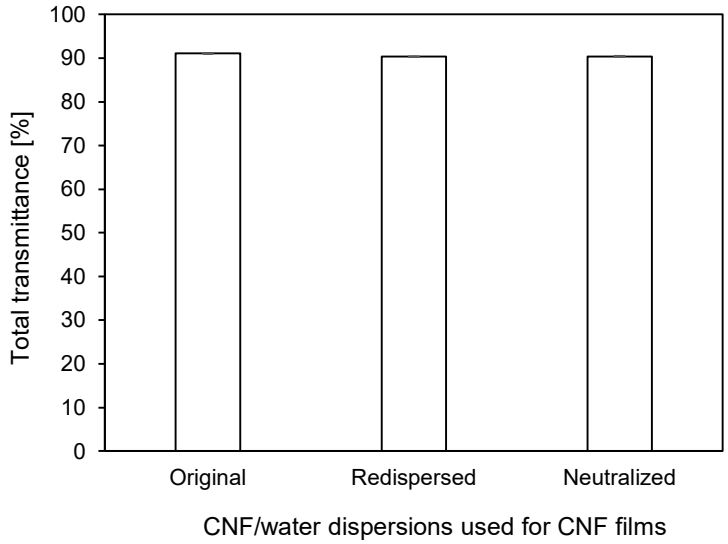

Figure 1-11. Total light transmittances of CNF films prepared from the original, redispersed, and neutralized CNF/water dispersions.

1.4 Conclusions

Electrodeposition is a promising dehydration method for CNFs. For dilute CNF/water dispersions, dehydration by electrodeposition was much more efficient than evaporation. Interestingly, the hierarchical structures of the CNFs after electrodeposition varied with the applied voltage. In addition, the concentrated CNF hydrogels were reused with neutralization and homogenization processes, and clear, transparent films were prepared. In a limitation of electrodeposition, it was found that a long time was required to achieve a CNF/water dispersion with a concentration above 2 wt%. Further studies are needed to increase the concentration, such as by applying a higher voltage or changing the

distance between electrodes according to the degree of dehydration. In the future, the effect of the type of CNFs also needs to be examined. While this method is effective for highly charged and nano-sized CNFs, such as TEMPO-oxidized CNFs, it might have limited effect on less charged and micro-sized cellulose fibers, such as microfibrillated cellulose (MFCs). These results provide new insights into dehydration via electrodeposition and the use of electrodeposition for hierarchical control of CNF structures.

1.5 References

1. Abe, K.; Iwamoto, S.; Yano, H. Obtaining Cellulose Nanofibers with a Uniform Width of 15 nm from Wood. *Biomacromolecules* **2007**, *8* (10), 3276–3278.
2. Isogai, A.; Saito, T.; Fukuzumi, H. TEMPO-Oxidized Cellulose Nanofibers. *Nanoscale* **2011**, *3* (1), 71–85.
3. Yang, X.; Reid, M. S.; Olsén, P.; Berglund, L. A. Eco-Friendly Cellulose Nanofibrils Designed by Nature: Effects from Preserving Native State. *ACS Nano* **2020**, *14* (1), 724–735.
4. Nemoto, J.; Saito, T.; Isogai, A. Simple Freeze-Drying Procedure for Producing Nanocellulose Aerogel-Containing, High-Performance Air Filters. *ACS Appl. Mater. Interfaces* **2015**, *7* (35), 19809–19815.
5. Kasuga, T.; Yagyu, H.; Uetani, K.; Koga, H.; Nogi, M. "Return to the Soil" Nanopaper Sensor Device for Hyperdense Sensor Networks. *ACS Appl. Mater. Interfaces* **2019**, *11* (46), 43488–43493.
6. Zhu, L.; Li, X.; Kasuga, T.; Uetani, K.; Nogi, M.; Koga, H. All-Cellulose-Derived Humidity Sensor Prepared via Direct Laser Writing of Conductive and Moisture-Stable Electrodes on TEMPO-Oxidized Cellulose Paper. *J. Mater. Chem. C* **2022**, *10* (10), 3712–3719.
7. Sakuma, W.; Yamasaki, S.; Fujisawa, S.; Kodama, T.; Shiomi, J.; Kanamori, K.; Saito, T. Mechanically Strong, Scalable, Mesoporous Xerogels of Nanocellulose Featuring Light Permeability, Thermal Insulation, and Flame Self-Extinction. *ACS Nano* **2021**, *15* (1), 1436–1444.
8. Sakuma, W.; Fujisawa, S.; Berglund, L. A.; Saito, T. Nanocellulose Xerogel as Template for Transparent, Thick, Flame-Retardant Polymer Nanocomposites. *Nanomaterials* **2021**, *11* (11), 3032.
9. Li, Q.; Hatakeyama, M.; Kitaoka, T. Bioadaptive Porous 3D Scaffolds Comprising Cellulose and Chitosan Nanofibers Constructed by Pickering Emulsion Templating. *Adv. Funct. Mater.* **2022**, *32* (22), 2200249.
10. Huang, Y.; Kasuga, T.; Nogi, M.; Koga, H. Clearly Transparent and Air-Permeable Nanopaper with Porous Structures Consisting of TEMPO-Oxidized Cellulose Nanofibers. *RSC Adv.* **2023**, *13* (31), 21494–21501.
11. Kasuga, T.; Mizui, A.; Koga, H.; Nogi, M. Wirelessly Powered Sensing Fertilizer for Precision

and Sustainable Agriculture. *Adv. Sustainable Syst.* **2023**, 2300314.

12. Lasseuguette, E.; Roux, D.; Nishiyama, Y. Rheological Properties of Microfibrillar Suspension of TEMPO-Oxidized Pulp. *Cellulose* **2008**, *15* (3), 425–433.

13. Isobe, N.; Kasuga, T.; Nogi, M. Clear Transparent Cellulose Nanopaper Prepared from a Concentrated Dispersion by High-Humidity Drying. *RSC Adv.* **2018**, *8* (4), 1833–1837.

14. Kasuga, T.; Isobe, N.; Yagyu, H.; Koga, H.; Nogi, M. Clearly Transparent Nanopaper from Highly Concentrated Cellulose Nanofiber Dispersion Using Dilution and Sonication. *Nanomaterials* **2018**, *8* (2), 104.

15. Li, C.; Kasuga, T.; Uetani, K.; Koga, H.; Nogi, M. High-Speed Fabrication of Clear Transparent Cellulose Nanopaper by Applying Humidity-Controlled Multi-Stage Drying Method. *Nanomaterials* **2020**, *10* (11), 2194.

16. Sinquefield, S.; Ciesielski, P. N.; Li, K.; Gardner, D. J.; Ozcan, S. Nanocellulose Dewatering and Drying: Current State and Future Perspectives. *ACS Sustainable Chem. Eng.* **2020**, *8* (26), 9601–9615.

17. Yagyu, H.; Kasuga, T.; Ogata, N.; Koga, H.; Daicho, K.; Goi, Y.; Nogi, M. Evaporative Dry Powders Derived from Cellulose Nanofiber Organogels to Fully Recover Inherent High Viscosity and High Transparency of Water Dispersion. *Macromol. Rapid Commun.* **2023**, *44* (17), 2300186.

18. Zhao, M.; Ansari, F.; Takeuchi, M.; Shimizu, M.; Saito, T.; Berglund, L. A.; Isogai, A. Nematic Structuring of Transparent and Multifunctional Nanocellulose Papers. *Nanoscale Horiz.* **2017**, 3 (1), 28–34.

19. Guccini, V.; Yu, S.; Agthe, M.; Gordeyeva, K.; Trushkina, Y.; Fall, A.; Schütz, C.; Salazar-Alvarez, G. Inducing Nematic Ordering of Cellulose Nanofibers Using Osmotic Dehydration. *Nanoscale* **2018**, *10* (48), 23157–23163.

20. Sheng, J.; Yang, R. A Facile Method to Concentrate Cellulose Nanofibril Slurries. *Cellulose* **2019**, *26* (2), 679–682.

21. Sekine, Y.; Nankawa, T.; Yunoki, S.; Sugita, T.; Nakagawa, H.; Yamada, T. Eco-Friendly Carboxymethyl Cellulose Nanofiber Hydrogels Prepared via Freeze Cross-Linking and Their Applications. *ACS Appl. Polym. Mater.* **2020**, *2* (12), 5482–5491.

22. Zhai, L.; Kim, H. C.; Kim, J. W.; Kim, J. Simple Centrifugal Fractionation to Reduce the Size

Distribution of Cellulose Nanofibers. *Sci. Rep.* **2020**, *10* (1), 1–8.

23. Wilson, B. P.; Yliniemi, K.; Gestranius, M.; Hakalahti, M.; Putkonen, M.; Lundström, M.; Karppinen, M.; Tammelin, T.; Kontturi, E. Structural Distinction Due to Deposition Method in Ultrathin Films of Cellulose Nanofibres. *Cellulose* **2018**, *25* (3), 1715–1724.

24. Kim, H.; Endrődi, B.; Salazar-Alvarez, G.; Cornell, A. One-Step Electro-Precipitation of Nanocellulose Hydrogels on Conducting Substrates and Its Possible Applications: Coatings, Composites, and Energy Devices. *ACS Sustainable Chem. Eng.* **2019**, *7* (24), 19415–19425.

25. Guo, X.; Gao, H.; Zhang, J.; Zhang, L.; Shi, X.; Du, Y. One-Step Electrochemically Induced Counterion Exchange to Construct Free-Standing Carboxylated Cellulose Nanofiber/Metal Composite Hydrogels. *Carbohydr. Polym.* **2020**, 117464.

26. Kasuga, T.; Yagyu, H.; Uetani, K.; Koga, H.; Nogi, M. Cellulose Nanofiber Coatings on Cu Electrodes for Cohesive Protection against Water-Induced Short-Circuit Failures. *ACS Appl. Nano Mater.* **2021**, *12*, 41.

27. Kasuga, T.; Saito, T.; Koga, H.; Nogi, M. One-Pot Hierarchical Structuring of Nanocellulose by Electrophoretic Deposition. *ACS Nano* **2022**, *16* (11), 18390–18397.

28. Wetterling, J.; Sahlin, K.; Mattsson, T.; Westman, G.; Theliander, H. Electroosmotic Dewatering of Cellulose Nanocrystals. *Cellulose* **2018**, *25* (4), 2321–2329.

29. Karna, N. K.; Lidén, A.; Wohlert, J.; Theliander, H. Electroassisted Filtration of Microfibrillated Cellulose: Insights Gained from Experimental and Simulation Studies. *Ind. Eng. Chem. Res.* **2021**, *60* (48), 17663–17676.

30. Shimizu, M.; Saito, T.; Isogai, A. Water-Resistant and High Oxygen-Barrier Nanocellulose Films with Interfibrillar Cross-Linkages Formed through Multivalent Metal Ions. *J. Membr. Sci.* **2016**, *500*, 1–7.

31. Sone, A.; Saito, T.; Isogai, A. Preparation of Aqueous Dispersions of TEMPO-Oxidized Cellulose Nanofibrils with Various Metal Counterions and Their Super Deodorant Performances. *ACS Macro Lett.* **2016**, *5* (12), 1402–1405.

32. Besra, L.; Uchikoshi, T.; Suzuki, T. S.; Sakka, Y. Experimental Verification of pH Localization Mechanism of Particle Consolidation at the Electrode/Solution Interface and Its Application to Pulsed DC Electrophoretic Deposition (EPD). *J. Eur. Ceram. Soc.* **2010**, *30* (5), 1187–1193.

33. Hsieh, M. C.; Koga, H.; Suganuma, K.; Nogi, M. Hazy Transparent Cellulose Nanopaper. *Sci.*

Rep. **2017**, *7* (1), 1–7.

34. Saito, T.; Uematsu, T.; Kimura, S.; Enomae, T.; Isogai, A. Self-Aligned Integration of Native Cellulose Nanofibrils towards Producing Diverse Bulk Materials. *Soft Matter* **2011**, *7* (19), 8804–8809

Chapter 2: High-Speed Fabrication of Clear Transparent Cellulose Nanopaper by Applying Humidity-Controlled Multi-Stage Drying Method

2.1 Introduction

Cellulose nanopaper is composed of only cellulose nanofibers, which are mainly generated from wood.[1,2] The general procedure to produce cellulose nanopaper is as follows. First, the wood chips are purified and disintegrated into micro-sized cellulose pulp fibers, and the pulp fibers are then further mechanically nanofibrillated in water to obtain a cellulose nanofiber dispersion. Finally, the cellulose nanofiber dispersion is dried using evaporation or vacuum-filtration-assisted drying to prepare optically transparent cellulose nanopaper.[3] The type of cellulose nanofiber dispersion is the key factor controlling the transparency of the cellulose nanopaper. The dispersion containing coarse nanofibers of microfibrillated cellulose can be dried within 12 h by heating after filtration; however, the obtained nanopaper will be translucent because of its low sheet density.[4–6] In contrast, if the dispersion only contains fine nanofibers of cellulose microfibrils (2–4-nm wide) or bundles of cellulose microfibrils (approximately 15-nm wide), a long drying time ranging from overnight to a few days is required.[1–3,7–19] For the case in which the dispersion only contains fine nanofibers, the obtained nanopaper will be clear transparent with low haze.[7] This outcome is achieved because the fine nanofibers are densely packed, resulting in the absence of cavities and thus preventing light from scattering inside the sheet.[1]

Because the properties of translucent nanopaper prepared in a short drying time are equivalent to those of traditional opaque paper, their applications are limited to layer coatings or additives for traditional paper. In contrast, transparent cellulose nanopaper, which requires a long drying time, offers various improved properties relative to those of translucent nanopaper, traditional paper, and certain polymer films. These improved properties include clear transparency, surface smoothness, high dielectric constant, and electrical insulation.[20–22] In the near future, flexible electronics will be applied owing to their excellent electrical and optical performance. Compared with traditional fossil-based materials, such as plastic films, transparent cellulose nanopaper is one of the best candidates for future flexible electronic substrates including solar cells, memory, transparent electrodes, sensors, and transistors.[12,19,22–24] Although various drying processes were developed over the past few years, rapid drying processes do not yet meet the desired standards. For the realization of these future applications, an in-depth understanding of the correlation between the moisture evaporation of dispersions and the cellulose nanopaper microstructure is necessary.

The drying mechanism of transparent cellulose nanopaper from fine cellulose nanofiber dispersions was recently investigated. Traditionally, the two main drying routes were vacuum-filtration-assisted drying, in which the dispersion is vacuum filtrated and the obtained wet sheet is heated using a hot press or oven drying,[1–3,7] and evaporation drying, in which the dispersion is dropped onto a flat substrate and then heated via oven drying.[3,8–19] Evaporation drying produces cellulose nanopaper with relatively superior mechanical properties, optical transparency, and gas barrier properties as well as high heat-transfer properties and electrical resistivity owing to the nematic-ordered and densely packed arrangement of nanofibers.[3] Although evaporation drying resulted in more desirable properties, it comes at the expense of drying time. Moreover, during evaporation drying, high humidity improves the transparency of the nanopaper; however, it also prolongs the drying time.[18]

In this work, I report that the drying time of cellulose nanopaper can be reduced while maintaining its clear transparency by controlling the drying condition. The essential requirement for clear transparency is the use of a fine cellulose nanofiber dispersion. As a typical type of fine cellulose nanofibers of cellulose microfibrils that can be easy to disperse in water homogeneously, TEMPO (2,2,6,6-tetramethylpiperidine-1-oxyl radical)-oxidized cellulose nanofibers (3–5-nm wide) [25,26] were used as the starting materials for the transparent cellulose nanopaper. The transparent cellulose nanopaper was prepared using evaporation drying. During the drying process, the dispersion weight change was monitored to understand the evaporation mechanism. After drying, the haze and density of the cellulose nanopaper were measured to investigate its microstructure. On the basis of these findings, this chapter proposed a humidity-controlled multi-stage drying method for transparent cellulose nanopaper to reduce the drying time while maintaining its clear transparency.

2.2 Experimental Section

2.2.1 Preparation of Cellulose Nanofiber Dispersion

The TEMPO (2,2,6,6-tetramethylpiperidine-1-oxyl radical)-oxidized cellulose nanofiber dispersion (RHEOCRYSTA I-2SX, DKS Co., Ltd., Kyoto, Japan) was used as a starting material. The 2 wt % RHEOCRYSTA I-2SX dispersion was diluted to 0.5 wt % and then stirred for 30 min. To remove the nanofiber aggregations, the diluted dispersion was passed 10 times at 245 MPa through a high-pressure water-jet system (Star Burst, HJP-25008, Sugino Machine Co., Ltd., Toyama, Japan) equipped with a ball-collision chamber. The obtained 0.45 wt % dispersion was then degassed using a centrifugal mixer (ARV-310, Thinky Corp., Tokyo, Japan), as shown in **Figure 2-1**.

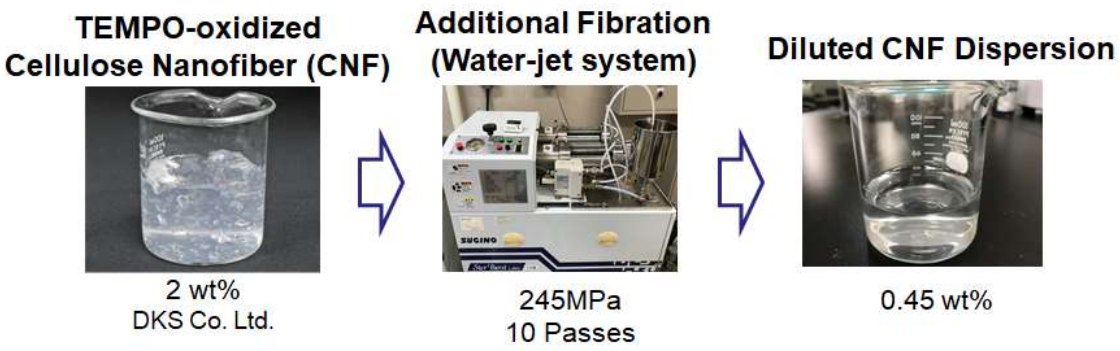

Figure 2-1. Preparation of cellulose nanofiber dispersion.

2.2.2 Preparation of Cellulose Nanopaper by Evaporation Drying

The conditioned dispersion (0.45 wt %, 22 g) was dropped evenly into a petri dish (9 cm diameter) silane-treated with decyltrimethoxysilane (KBM-3103, Shin-Etsu Chemical Co., Ltd., Tokyo, Japan) and was then dried at various temperatures (ranging from 45 °C to 85 °C) and relative humidities (ranging from 35% to 75%) in an environmental chamber (SH-642, ESPEC Corp., Osaka, Japan), as shown in **Figure 2-2**.

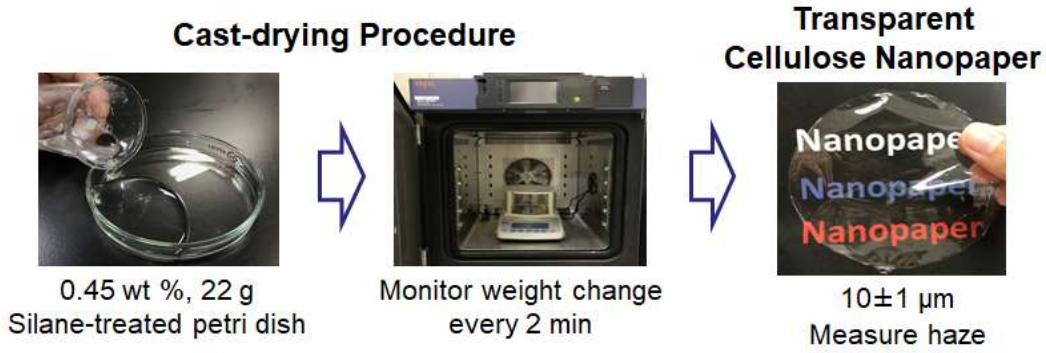

Figure 2-2. Preparation of cellulose nanopaper.

2.2.3 Air Flow System in a Conventional Oven

The air flow system used in this work was a flat air nozzle (AFTCS15, MISUMI Group Inc., Tokyo, Japan) with 13 orifices of 9 mm diameter connected to an air compressor (PC3-5.5TL, YAEZAKI KŪATSU Co., Ltd., Tokyo, Japan). The system softly blew air (air flow rate: 0.4–0.5 L/min) toward the dispersion to remove the saturated water vapor at the water/air interface (**Figure 2-3**). When the air flow system was blowing, the RH directly above the water/air interface was reduced, thus increasing

the evaporation rate.

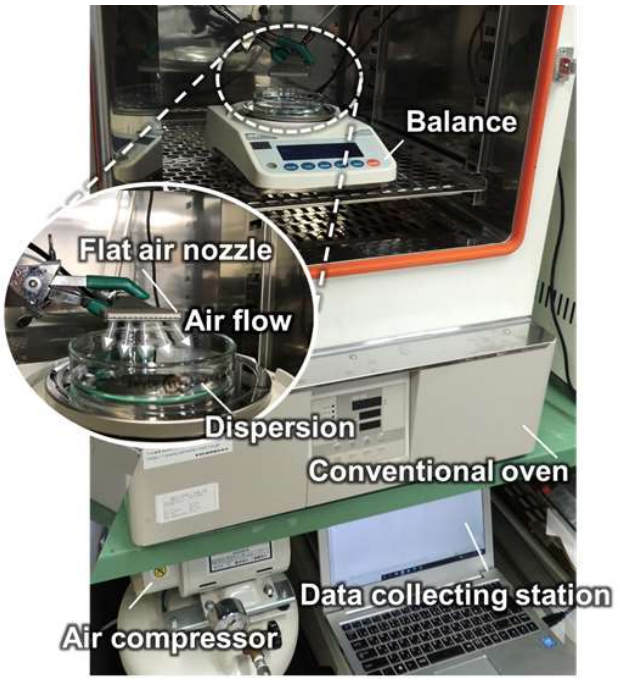

Figure 2-3. The air flow system used to control humidity in a conventional oven.

2.2.4 Characterization

Observation by Field Emission Scanning Electron Microscopy

The diluted TEMPO-oxidized cellulose nanofiber dispersion was dried first, and then was coated by platinum using an ion sputtering device (E-1045, Hitachi High-Tech Science Corp., Tokyo, Japan). The nanofibers were observed by a field-emission scanning electron microscope (FE-SEM, SU-8020, Hitachi High-Tech Science Corp., Tokyo, Japan).

Weight Monitoring and Drying Time Determination

After 30 min of pre-drying, the weight change of the dispersion was monitored using a balance (FX-300i, A&D Co., Ltd., Tokyo, Japan) that placed in the environmental chamber (SH-642, ESPEC Corp., Osaka, Japan) every 2 min. After the weight remained constant at approximately 0.1 g (the weight of the nanopaper) and stopped changing for more than 30 min, the drying procedure was considered complete. The end of the drying time was considered the time at which the dried weight changed less than 0.045%.

Thickness Measurement

The thickness of the obtained nanopaper was measured by a digital thickness gauge (G2-205M, Ozaki Mfg Co., Ltd., Tokyo, Japan) at 10 different spots for calculating the average value.

Transmittance and Haze Measurement

Total transmittance of the obtained nanopaper was measured by a UV-vis-NIR spectrophotometer (UV-3600 Plus, Shimadzu Corp., Kyoto, Japan).

The haze of the obtained nanopaper with thickness of 10±1 μm was measured by a haze meter (HZ-V3, Suga Test Instruments Co., Ltd., Tokyo, Japan). The haze obtained from the haze meter was calculated from the following equation by the machine automatically (**Figure 2-4**).

$$Haze\ [\%] = Td/Tt \times 100$$

T_d: Diffuse transmittance (%)

Tt: Total transmittance (%)

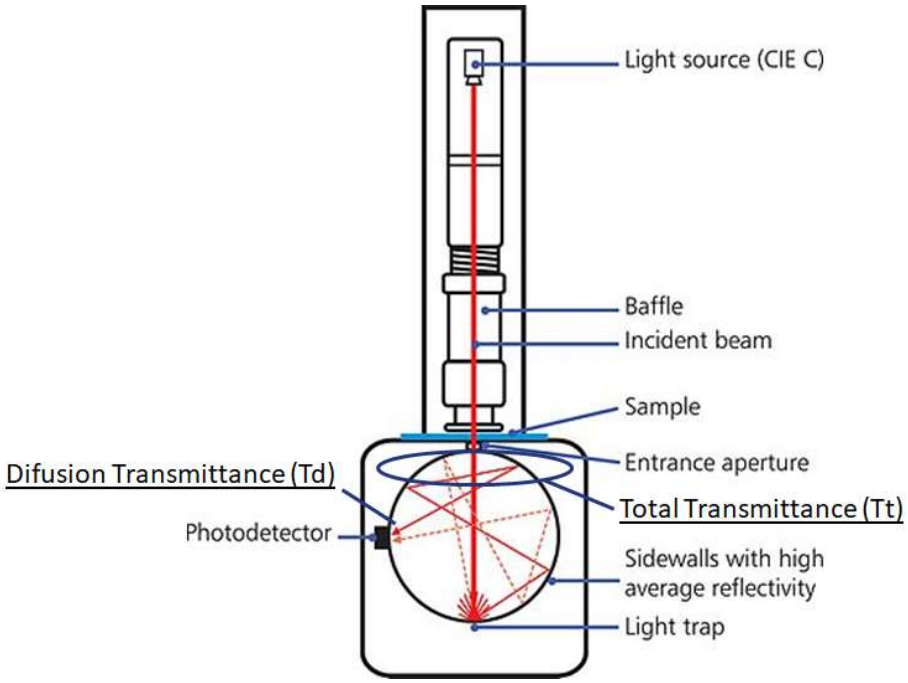

Figure 2-4. Schematic of haze meter measurement.

Crystallinity Index Measurement

X-ray diffraction (XRD) patterns were recorded using a Rigaku MiniFlex600 (Tokyo, Japan) with Cu–Kα radiation and a scanning angle (2θ) range of 5–40° at 40 kV voltage and 15 mA current. The crystallinity index of cellulose I was calculated from the (200) reflection (2θ = ca. 22.6°).[14, 27]

Surface Roughness Measurement

The surface roughness of the nanopaper was determined using an atomic force microscope (AFM, Nanocute, SII Nano Technology Inc., Chiba, Japan) in the dynamic force mode (measurement range: 10 μm × 10 μm).

Apparent Density Measurement

The obtained nanopaper sample (~50 mg) was placed into weighing bottle and dried under vacuum at 105 °C for 3 h for further density analyzing. The weight of the sample was measured by an analytical balance with an accuracy of ±0.03 mg for 100 g (BM-252, A&D Co., Ltd., Tokyo, Japan).

The apparent density was analyzed using a BELPycno helium pycnometer (Bonsai Advanced Technologies SL., Madrid, Spain). The weight-measured nanopaper was placed into the chamber with a volume of 1 cm^3 and exposed to a vacuum (~0.5 kPa). Then helium gas was purged 30 times at 145 kPa. The density was measured at 25 ± 0.1 °C when no change of over 0.06 kPa for 30 s was observed. The measurement was repeated until a standard deviation of less than 0.5% was achieved for 30 consecutive measurements, and finally the average of the last five measurements was taken as the density of the nanopaper.[28]

2.3 Results and Discussion

2.3.1 Key Parameters for Fabrication Time and Haze of Cellulose Nanopaper

Cellulose Nanopaper Dried in Extreme Temperature

In this study, 3–5-nm wide TEMPO-oxidized cellulose nanofibers (**Figure 2-5**) was used for preparing cellulose nanopaper. When such fine nanofibers are homogeneously dispersed in water, their concentration is usually adjusted to less than 1 wt% because of their high viscosity. Therefore, it took 12 h at 50 °C using evaporation drying to produce 10-μm-thick cellulose nanopaper (**Figure 2-6 a**). The simplest way to reduce the drying time is to increase the drying temperature. In the extreme case,

when the dispersion was heated at 110 °C, the nanopaper was produced in only 2 h. However, when the dispersion was heated at a temperature higher than the boiling point of water, the obtained nanopaper contained many air bubbles (**Figure 2-6 b**). From these experiments, it was apparent that drying above the boiling point dramatically reduced the drying time but adversely affected the transparency.

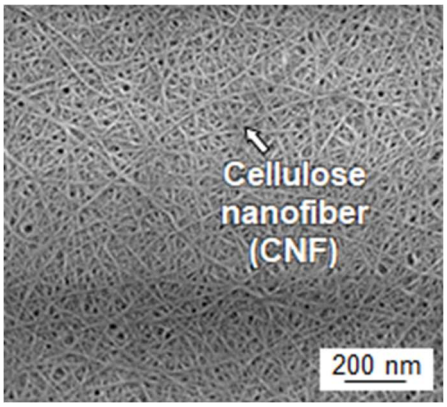

Figure 2-5. FE-SEM micrographs of TEMPO-oxidized cellulose nanofibers.

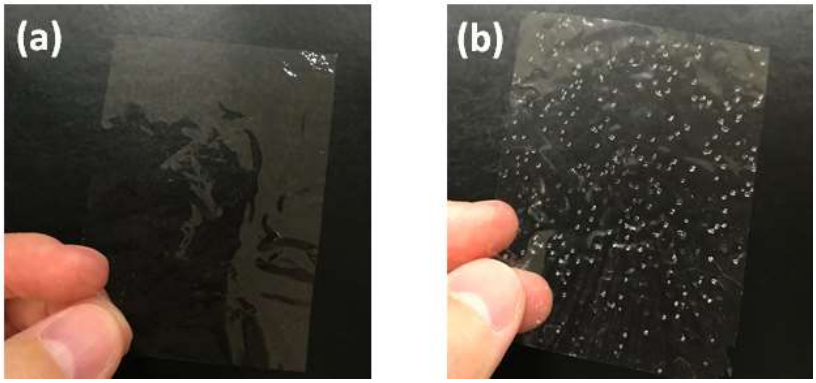

Figure 2-6. Appearance of transparent cellulose nanopaper prepared using evaporation drying at **a**) 50 °C for 12 h and **b**) 110 °C for 2 h.

The Effect of Drying Temperature and Relative Humidity (RH)

To produce low-haze cellulose nanopaper in a short drying time, the temperature and humidity must be carefully designed during the drying process. It is well known that for the same amount of water vapor, when the atmospheric temperature is increased in a closed system, the absolute humidity remains constant but the relative humidity (RH) decreases. Because the moisture evaporation is affected by not only the temperature but also the RH, the effect of temperature and humidity should be separately discussed when the drying schedule is determined. Therefore, the cellulose nanofiber

dispersion was dried using an environmental chamber that enabled independent control of the ambient temperature (45–85 °C) and RH (35–75%).

Although these two factors can both affect the drying time, the RH plays a more important role in determining the haze of the nanopaper. At each temperature, a lower RH reduced the drying time (**Figure 2-7 a**). For example, at 65 °C, decreasing the RH from 75% to 35% reduced the drying time from 17.7 h to 6.7 h. In contrast, at each temperature, a lower RH increased the haze (**Figure 2-7 b**). For example, at 65 ˚C, decreasing the RH from 75% to 35% increased the haze from 0.65% to 0.99%. These results indicate that a short drying time requires a lower RH, whereas lower haze requires a higher RH. Therefore, these contradictory humidity conditions must be taken into account to reduce both the drying time and haze.

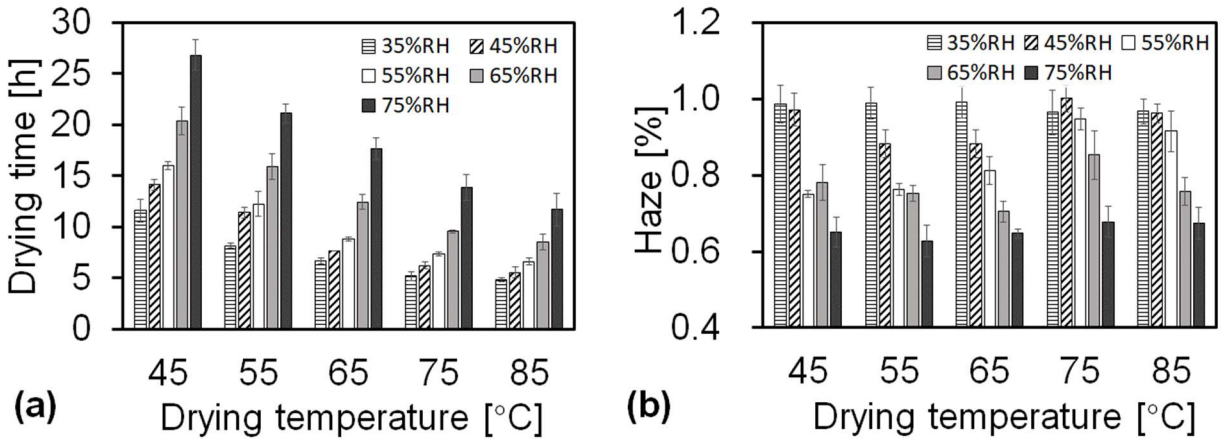

Figure 2-7. Drying time of nanofiber dispersions (0.45 wt%, 22 g) and haze of nanopaper with 10 ± 1 μm thickness under various temperature and humidity conditions. **a**) Drying time and **b**) haze as a function of drying temperature.

2.3.2 New Humidity-Regulated Multi-Stage Drying Method

Understanding of Drying Behavior of Cellulose Nanopaper

Before the contradictory humidity conditions required to achieve the optimal drying time and haze could be discussed, the drying behavior needed to be thoroughly understood. While drying the dispersions, their appearance drastically changed (**Figure 2-8**). The sample before drying was liquid-like at a concentration of 0.45 wt%, and it maintained a liquid-like appearance until the concentration increased to 0.85 wt%. However, as the water evaporation proceeded, the sample became paste-like at approximately 10 wt% and finally became solid at approximately 100 wt%. These appearance changes

have a close relationship with the concentration as well as the drying rate.

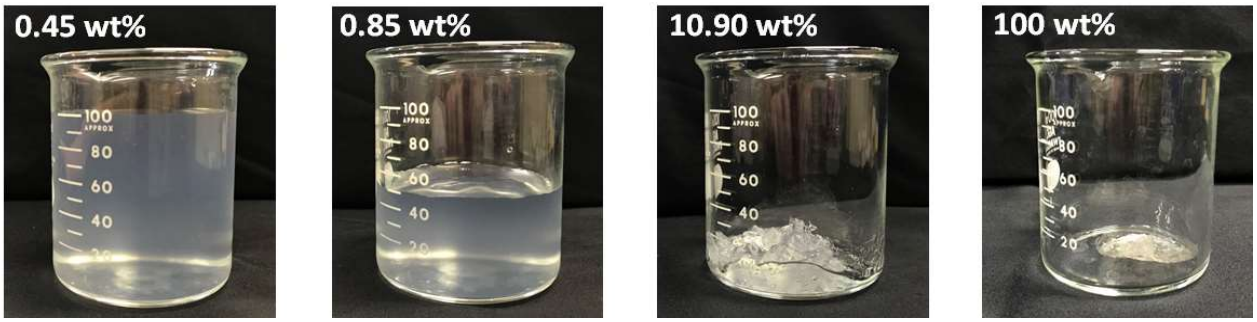

Figure 2-8. Change of appearance of cellulose nanofiber dispersion during drying.

The concentration change is plotted as a function of the drying time at 55 °C and 55% RH in **Figure 2-9 a**. The concentration linearly increased when the sample was liquid-like (until approximately 8 h), whereas the concentration exponentially increased after the sample became paste-like (from approximately 8 h).

These appearance changes also reflect the drying rate (**Figure 2-9 b**). For the liquid-like state (until approximately 8 h), the water evaporation occurred at the sample surface because the surface was rich in water. Therefore, the drying rate was constant during this period, which is denoted as the constant-drying-rate period. When the sample turned paste-like (from approximately 8 h), mainly the internal water of the sample evaporated. The evaporation interface proceeded further inward to the sample body with extended drying time; therefore, the drying rate decreased, and this period is denoted the falling-drying-rate period. **Table 2-1** summarizes the three drying times (total drying time, constant-drying-rate-period time, and falling-drying-rate-period time), the transit concentration from the constant-drying-rate period to the falling-drying-rate period, and the haze of the obtained cellulose nanopaper for all the drying conditions. For transparent cellulose nanopaper, haze is strongly dependent on the internal microstructure, more specifically, the packing of nanofibers with different density. [7] Therefore, the haze might be controlled in the falling-drying-rate period, during which the water evaporation occurred inside the nanopaper and affected the packing of nanofibers.

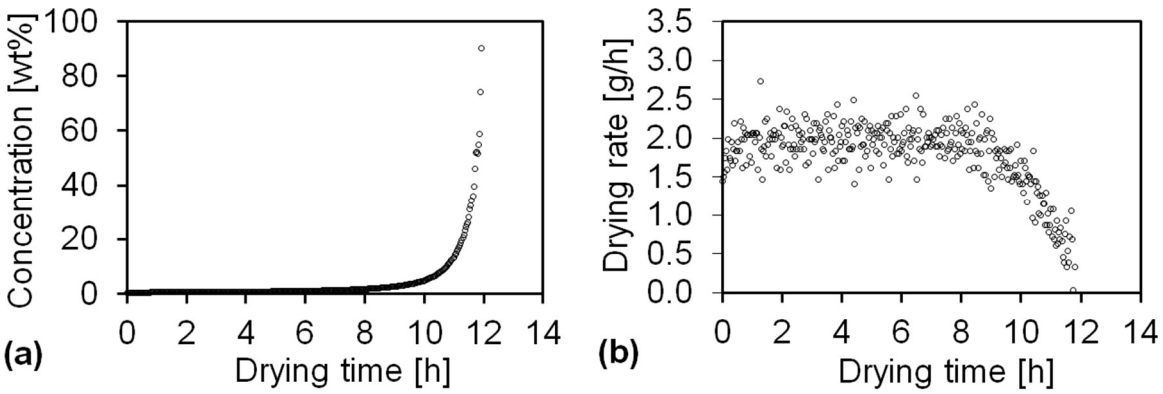

Figure 2-9. (**a**) Dispersion concentration and (**b**) drying rate change as a function of drying time at 55 °C and 55% RH.

Table 2-1 Drying time, transit concentration (the dispersion transit from constant drying rate period to falling drying rate period), and haze of obtained cellulose nanopaper.

Relative humidity	Temperature [˚C]	Total drying time [h]	Constant drying rate period		Falling drying rate period		Transit concentration [wt %]	Haze [%]
			Period time [h]	Ratio [%]	Period time [h]	Ratio [%]		
RH 35%	45	12.8	9.3	73	3.5	27	2.45	1.00
RH 35%	55	8	5.7	71	2.3	29	2.32	1.02
RH 35%	65	6.3	4.8	76	1.5	24	2.52	1.00
RH 35%	75	5.3	3.7	70	1.6	30	2.46	0.96
RH 35%	85	4.5	3.3	73	1.2	27	2.38	0.99

Relative humidity	Temperature[˚C]	Total drying time [h]	Constant drying rate period		Falling drying rate period		Transit concentration [wt %]	Haze [%]
			Period time [h]	Ratio [%]	Period time [h]	Ratio [%]		
RH 45%	45	14.6	11.6	79	3.0	21	3.96	0.94
RH 45%	55	11.7	8.4	72	3.3	28	3.72	0.85
RH 45%	65	7.6	5.9	78	1.5	22	3.34	0.91
RH 45%	75	5.8	4.7	81	1.6	19	3.97	0.98
RH 45%	85	5	3.9	78	1.2	22	4.35	0.95

Relative humidity	Temperature [˚C]	Total drying time [h]	Constant drying rate period		Falling drying rate period		Transit concentration [wt %]	Haze [%]
			Period time [h)	Ratio [%]	Period time [h]	Ratio [%]		
RH 55%	45	16.3	13.9	85	2.4	15	4.27	0.75
RH 55%	55	12.1	10.4	86	1.7	14	4.08	0.76
RH 55%	65	8.6	6.8	79	1.8	21	4.07	0.78

RH 55%	75	7.1	5.8	82	1.3	18	3.46	0.93
RH 55%	85	4.5	3.3	73	1.2	27	2.38	0.91

Relative humidity	Temperature [˚C]	Total drying time [h]	Constant drying rate period		Falling drying rate period		Transit concentration [wt %]	Haze [%]
			Period time [h]	Ratio [%]	Period time [h]	Ratio [%]		
RH 65%	45	18.9	15.9	84	3.0	16	4.6	0.82
RH 65%	55	14.5	12.7	88	1.8	12	4.75	0.78
RH 65%	65	12.9	11.0	85	1.9	15	4.72	0.73
RH 65%	75	9.7	7.9	81	1.8	19	4.06	0.88
RH 65%	85	8	6.5	81	1.5	19	4.61	0.74

Relative humidity	Temperature [˚C]	Total drying time [h]	Constant drying rate period		Falling drying rate period		Transit concentration [wt %]	Haze [%]
			Period time [h]	Ratio [%]	Period time [h]	Ratio [%]		
RH 75%	45	25.2	23.7	94	1.5	6	9.33	0.61
RH 75%	55	20.4	18.9	93	1.5	7	8.72	0.67
RH 75%	65	17.5	15.3	87	2.2	13	6.98	0.64
RH 75%	75	12.8	11.5	90	1.3	10	7.28	0.72
RH 75%	85	11.3	10.1	89	1.2	11	7.82	0.67

The Effect of RH on Nanopaper's Haze during Falling-Drying-Rate Period

To overcome the contradictory humidity conditions required to optimize the drying time and haze of cellulose nanopaper, the effect of the RH on the haze during the falling-drying-rate period was evaluated. In these experiments, the drying temperature was set at a constant value of 55 °C while the RH was set at 55% during the constant-drying-rate period and 15%, 55%, or 85% during the falling-drying-rate period (**Figure 2-10 a**).

With the same high total transmittances (~90%) in the visible wavelength range of 400–800 (**Figure 2-11**) and similar high crystallinities (~80%) (**Figure 2-12**), there exists an interesting relationship between the RH in the falling-drying-rate period and the haze of the nanopaper (**Figure 2-10 b, bar**). The lowest RH of 15% produced the worst haze of the nanopaper of 1.00%. The RH of 55% got the better haze of 0.80%, and the highest RH of 85% resulted in the best haze of 0.71%. The haze was caused by light scattering inside or at the surface of the transparent nanopaper. The surface roughness (Rq) of the resultant nanopaper was about 3.3 nm, 2.9 nm, and 3.1 nm, respectively. Therefore, the variations of the obtained haze values were mainly caused by the different porosities of

nanopaper. The apparent density in these nanopaper showed a close relationship with the RH during the falling-drying-rate period (**Figure 2-10 b, dot**). When the RH increased in the falling-drying-rate period, the apparent densities in the nanopaper increased.

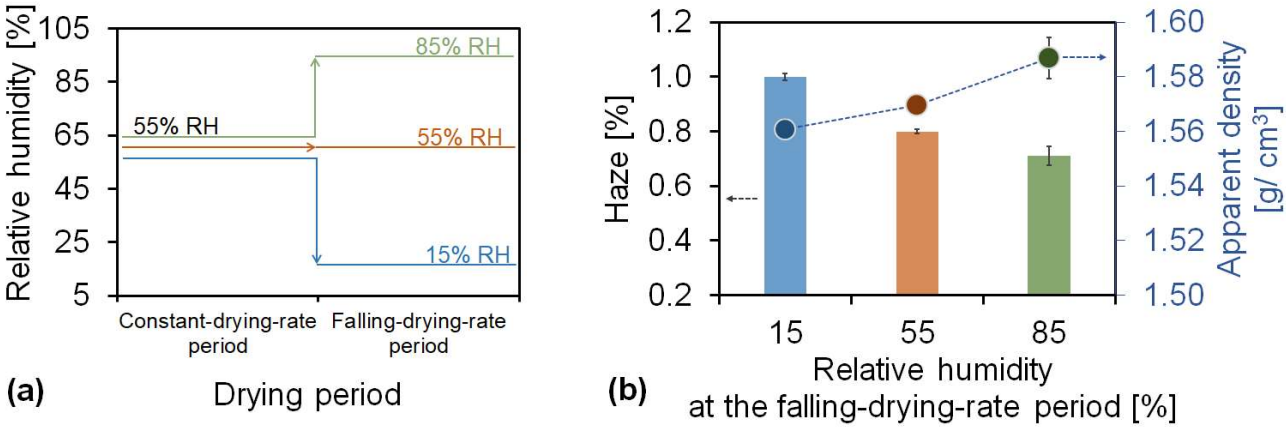

Figure 2-10. a) Drying strategy for investigation of the relationship between the haze and RH during the falling-drying-rate period. During the drying process, the temperature was 55 °C for the entire period, and the RH was 55% during the constant-drying-rate period and 15%, 55%, or 85% during the falling-drying-rate period; **b**) Corresponding haze (bar) and apparent density (dot) of cellulose nanopaper.

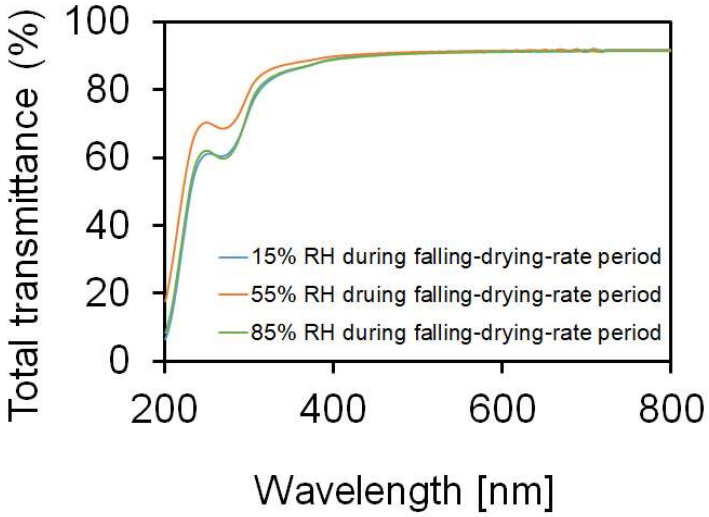

Figure 2-11. Total transmittance of cellulose nanopaper under different conditions.

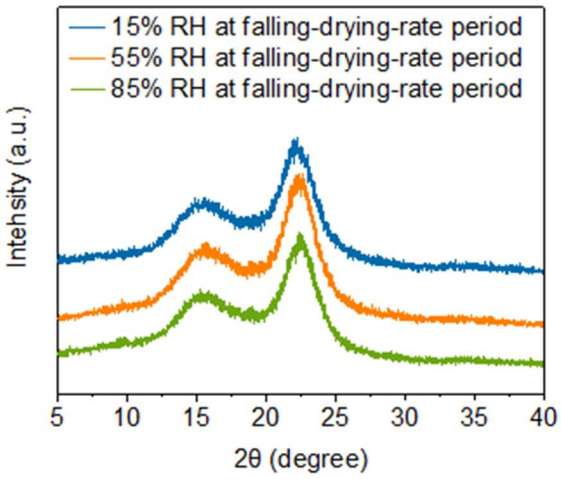

Figure 2-12. X-ray diffraction profiles of nanopaper dried under different conditions.

Hypothesis of Cellulose Nanofibers Assembly during Drying

These results in last section that a lower RH during the falling-drying-rate period accelerated water evaporation from inside the sample, and the inhomogeneous aggregation of the nanofibers during the quick fabrication resulted in the formation of more air voids inside the sample. However, a higher RH decelerated the water evaporation, which provided the slow formation of interactions between nanofibers, thus leading to less air voids remaining inside the sample (**Figure 2-13**). Therefore, to achieve low haze of the nanopaper, the RH should be higher during the falling-drying-rate period.

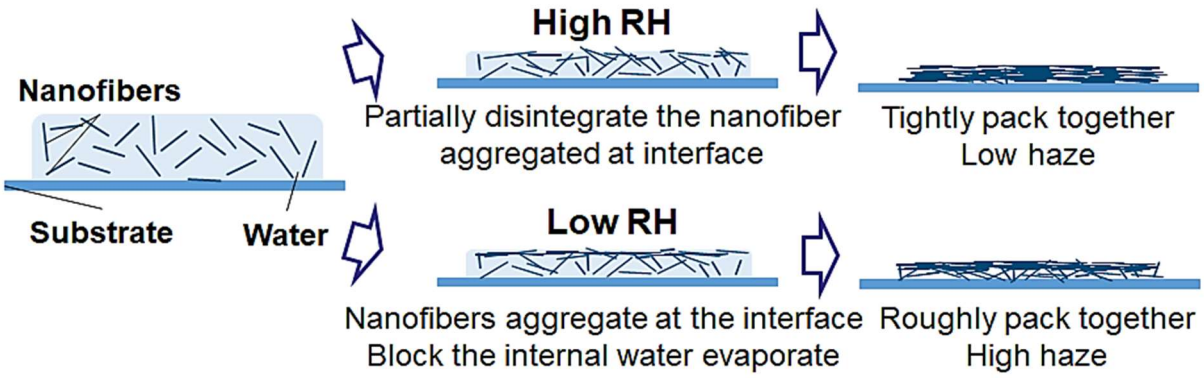

Figure 2-13. Schematic of cellulose nanofibers' assembling at different RH during falling-drying-rate period.

New Humidity-Regulated Multi-Stage Drying Method

From these results and discussion, it was apparent that a lower RH reduced the drying time during the constant-drying-rate period when the evaporation was mainly from the water-rich interface, and the subsequent higher RH during the falling-drying-rate period reduced the haze of the cellulose nanopaper when the evaporated water mainly came from inside the sample. Therefore, a new humidity-regulated multi-stage drying method was proposed. For this new drying method, the RH is kept low at constant-drying-rate period and then changed to higher RH for fast fabricating the cellulose nanopaper with superior optical properties (**Figure 2-14**).

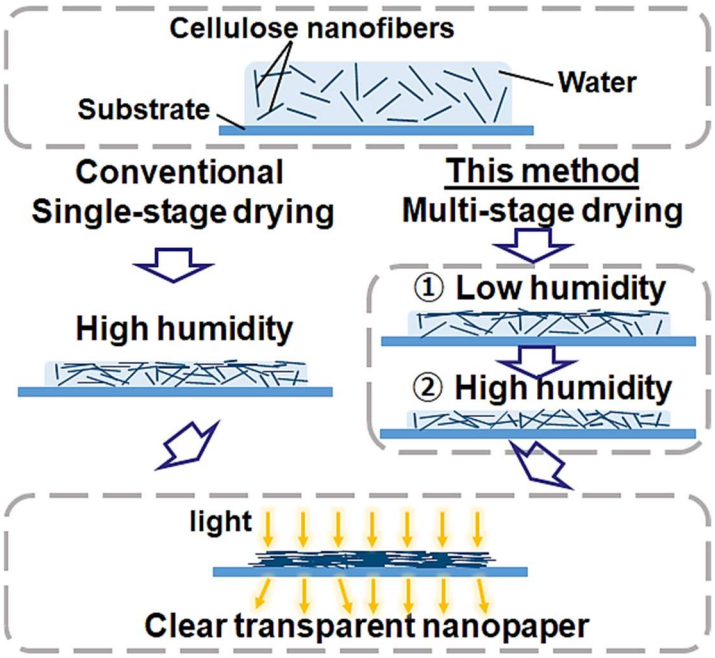

Figure 2-14. Schematic of a new humidity-regularized multi-stage drying method.

2.3.3 Applications

Humidity-Controllable Environmental Chamber

After clearly understanding the drying behavior of the nanopaper, reducing the drying time and haze of nanopaper was attempted in a humidity-controllable environmental chamber. Because the constant-drying-rate period accounts for 70–90% of the total drying time (**Table 2-1**), reducing the duration of this period is the most effective way to decrease the total drying time.

In these experiments, the drying temperature was set at 85 °C for the entire drying time, and the RH was set at 35% or 75% during the constant-drying-rate period and 75% during the falling-drying-

rate period (**Figure 2-15 a**). When the RH remained at 75% during both periods, as in the traditional single-stage drying process, the drying time was 11.7 h (**Figure 2-15 b, bar**). However, when the new multi-stage drying was applied with conditions of 35% RH during the constant-drying-rate period and 75% RH during the falling-drying-rate period, the drying time was only 7.6 h (**Figure 2-15 b, bar**), a decrease of 35%.

The RH during the different drying periods played different roles in determining the haze level. During the falling-drying-rate period, decreasing the RH led to deterioration of the haze of the cellulose nanopaper because the evaporation was mainly from the internal water of the film. In contrast, during the constant-drying-rate period, the water evaporation occurred mainly at the air/water interface of the dispersion. Therefore, even when the drying rate increased by applying a lower relative humidity (35%) during this period, the resulting cellulose nanopaper still maintained a low haze of 0.61%, which was comparable to the haze of 0.67% from that dried under a constant higher RH (75% in this case) with shorter drying time (**Figure 2-15 b, dot**). Therefore, this multi-stage drying method satisfies the contradictory humidity conditions required to reduce both the drying time and haze.

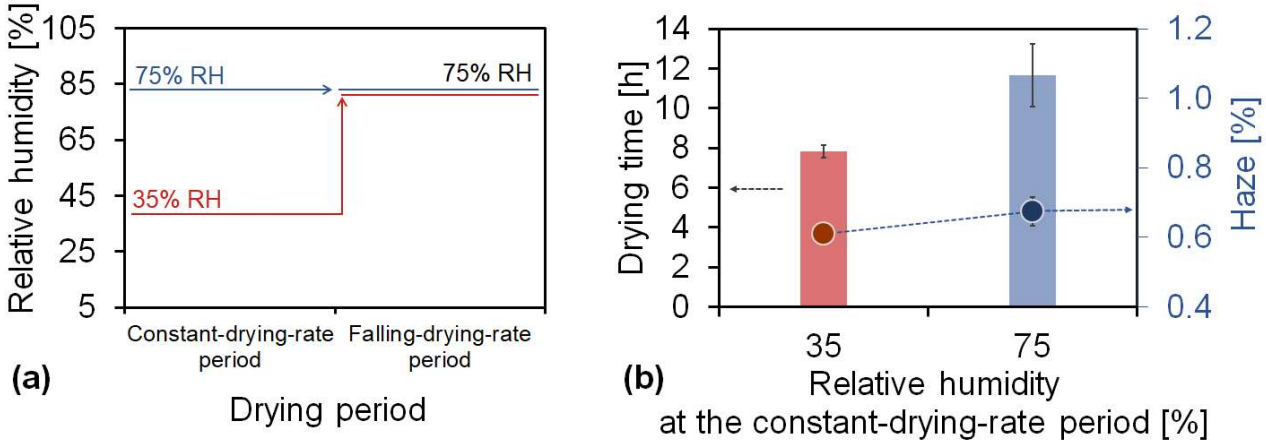

Figure 2-15. a) Drying strategy for investigation of the relationship between the haze and RH during constant-drying-rate period. **b**) Corresponding drying time (bar) and haze (dot) of cellulose nanopaper. During the drying process, the temperature was 85 °C for the entire period, and the RH was 35% or 75% during the constant-drying-rate period and 75% during the falling-drying-rate period.

Humidity-Uncontrollable Conventional Oven

To reduce the drying time of the dispersion and the haze of the cellulose nanopaper, a humidity-

controlled multi-stage drying process using an environmental chamber that can independently control the ambient temperature and RH was confirmed. However, in a conventional oven, only the temperature and not the humidity can be controlled, and the humidity inside the conventional oven is usually quite low. For example, the RH of a conventional oven is approximately 18% at 35 °C and 4% at 75 °C when the room temperature and RH are 20 °C and 70%, respectively. Therefore, achieving higher RH during the falling-drying-rate periods would be difficult using a conventional oven. Theoretically, the vapor pressure of the air vapor directly above the surface of the drying sample always remains approximately the saturated vapor pressure when water is evaporated from the sample. Air flow to the sample surface decreases the vapor pressure below the saturated vapor pressure, and air retention increases the vapor pressure back to the saturated vapor pressure (**Figure 2-16**).

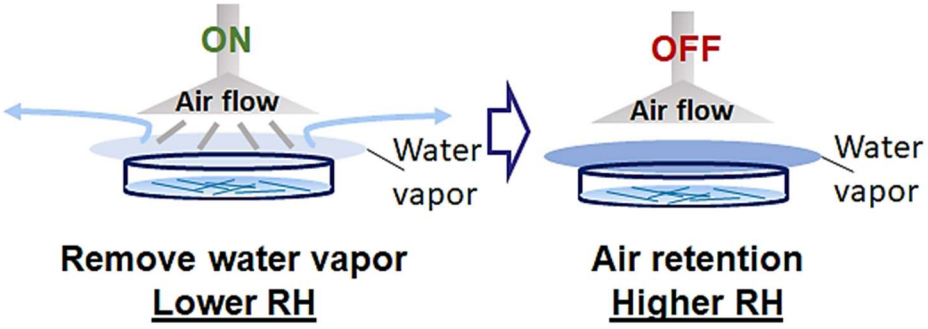

Figure 2-16. Schematic of RH controlled by air flow.

Therefore, an air flow system was developed in a conventional oven that enables control of the RH directly above the surface of the dispersion (**Figure 2-17, see also Figure 2-3**). When the air flow was not applied at 35 °C drying, the saturated vapor pressure was maintained at the dispersion surface during all the drying periods. As a result, transparent cellulose nanopaper with 0.64% haze was produced in 36.6 h (**Figure 2-18 a**). In contrast, when the air flow was applied only during the constant-drying-rate period at 35 °C drying, the vapor pressure of the dispersion surface became lower than the saturated vapor pressure, resulting in a faster drying rate and thus contributing to a shorter constant-drying-rate period; the saturated vapor pressure was maintained during the falling-drying-rate period to ensure dense packing. As a result, the total drying time decreased to 18.6 h while maintaining the haze of the transparent cellulose nanopaper at 0.65% (**Figure 2-18 a**). Moreover, when the air flow was applied only during the constant-drying-rate period at 75 °C drying, the total drying time decreased from 5.7 h to 3.8 h while maintaining the haze of the transparent cellulose nanopaper at approximately 1% (**Figure 2-18 b**).

These results suggest that the air flow during the constant-drying-rate period increased the drying rate and that the air retention during the falling-drying-rate period did not produce more air voids than usual. Therefore, the concept of a humidity-regulated multi-stage drying process can be applied not only in an environmental chamber, where the humidity can be controlled, but also in a conventional oven, where the humidity cannot be controlled.

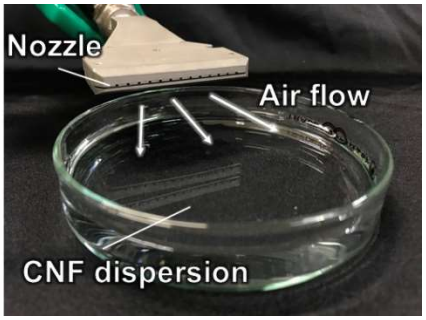

Figure 2-17. The air flow system softly blew toward the dispersion to remove the water vapor at the water/air interface.

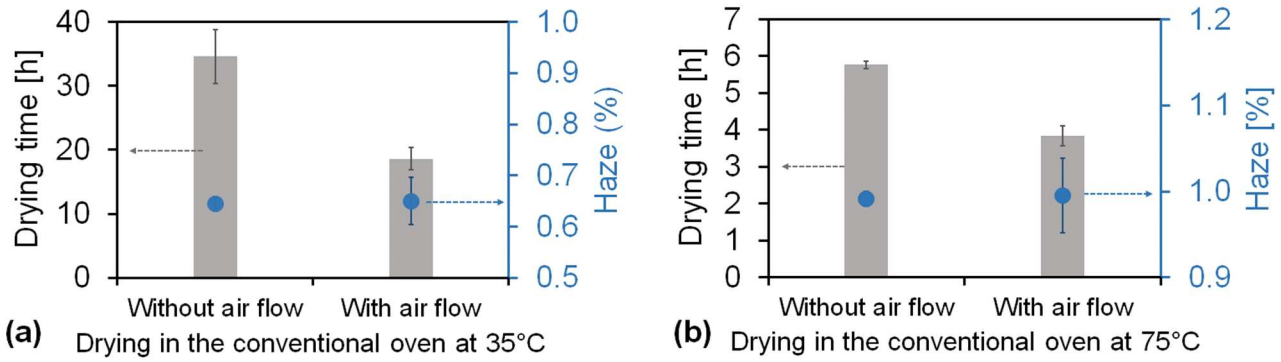

Figure 2-18. Drying time of the cellulose nanofiber dispersion and haze of the cellulose nanopaper in the conventional oven with and without the air flow system under **a**) 35 °C drying and **b**) 75 °C drying.

2.4 Conclusions

This work demonstrates the possibility of reducing the drying time of aqueous cellulose nanofiber dispersions while maintaining the low haze of the resulting cellulose nanopaper. When the dispersion was dried using an environmental chamber, the drying time and haze were observed to be more sensitive to the RH than to the temperature. However, reduction of the drying time and haze required contradictory humidity conditions. An increase in RH positively affected haze reduction but negatively

affected the drying time. From monitoring the weight change of the dispersion, it appeared that the drying procedure consisted of a constant-drying-rate period and a falling-drying-rate period. The RH could be kept lower during the constant-drying-rate period, which was related less to the microstructure of the nanopaper and more to its drying time because water evaporation during this period mainly occurred at the water-rich surface. For the falling-drying-rate period, the evaporated water was mainly from internal water, and a relatively higher RH during this period promoted the tight packing of cellulose nanofibers, resulting in a lower haze.

Other than the humidity-controllable environmental chamber, this humidity-regulated multi-stage drying process can also be applied in a conventional oven with the addition of a simple air flow system. Regardless of the oven type, the air above the surface of the sample always remained at the saturated vapor pressure, which inhibited the quick water evaporation. Therefore, when the air flow system was applied to the surface during the constant-drying-rate period, thus removing the water vapor above the surface, the total drying time was reduced to less than 4 h while maintaining the low haze.

This humidity-regulated multi-stage drying process demonstrated the effectiveness in the nanopaper preparation, and has a great potential for the widespread use of nanopaper-based flexible electronics.

2.5 References

1. Nogi, M.; Iwamoto, S.; Nakagaito, A. N.; Yano, H. Optically Transparent Nanofiber Paper. *Adv. Mater.* **2009**, *21* (15), 1595–1598.
2. Fukuzumi, H.; Saito, T.; Iwata, T.; Kumamoto, Y.; Isogai, A. Transparent and High Gas Barrier Films of Cellulose Nanofibers Prepared by TEMPO-Mediated Oxidation. *Biomacromolecules* **2009**, *10* (1), 162–165.
3. Zhao, M.; Ansari, F.; Takeuchi, M.; Shimizu, M.; Saito, T.; Berglund, L. A.; Isogai, A. Nematic Structuring of Transparent and Multifunctional Nanocellulose Papers. *Nanoscale Horiz.* **2018**, *3* (1), 28–34.
4. Sehaqui, H.; Liu, A.; Zhou, Q.; Berglund, L. A. Fast Preparation Procedure for Large, Flat Cellulose and Cellulose/Inorganic Nanopaper Structures. *Biomacromolecules* **2010**, *11* (8), 2195–2198.
5. Honorato, C.; Kumar, V.; Liu, J.; Koivula, H.; Xu, C.; Toivakka, M. Transparent Nanocellulose-Pigment Composite Films. *J. Mater. Sci*. **2015**, *50* (19), 7343–7352.
6. Chen, S.; Song, Y.; Xu, F. Highly Transparent and Hazy Cellulose Nanopaper Simultaneously with a Self-Cleaning Superhydrophobic Surface. *ACS Sustain. Chem. Eng*. **2018**, *6* (4), 5173–5181.
7. Hsieh, M. C.; Koga, H.; Suganuma, K.; Nogi, M. Hazy Transparent Cellulose Nanopaper. *Sci. Rep.* **2017**, *7*, 41590.
8. Siró, I.; Plackett, D.; Hedenqvist, M.; Ankerfors, M.; Lindström, T. Highly Transparent Films from Carboxymethylated Microfibrillated Cellulose: The Effect of Multiple Homogenization Steps on Key Properties. *J. Appl. Polym. Sci.* **2010**, *116* (5), 2658–2667.
9. Zhu, M.; Peng, X.; Wang, Z.; Bai, Z.; Chen, B.; Wang, Y.; Hao, H.; Shao, Z.; Zhong, H. Highly Transparent and Colour-Tunable Composite Films with Increased Quantum Dot Loading. *J. Mater. Chem. C* **2014**, *2* (38), 10031–10036.
10. Shimizu, M.; Saito, T.; Fukuzumi, H.; Isogai, A. Hydrophobic, Ductile, and Transparent Nanocellulose Films with Quaternary Alkylammonium Carboxylates on Nanofibril Surfaces. *Biomacromolecules* **2014**, *15* (12), 4320–4325.

11. Nogi, M.; Kim, C.; Sugahara, T.; Inui, T.; Takahashi, T.; Suganuma, K. High Thermal Stability of Optical Transparency in Cellulose Nanofiber Paper. *Appl. Phys. Lett.* **2013**, *102* (18), 181911.

12. Nogi, M.; Karakawa, M.; Komoda, N.; Yagyu, H.; Nge, T. T. Transparent Conductive Nanofiber Paper for Foldable Solar Cells. *Sci. Rep.* **2015**, *5*, 17254.

13. Yagyu, H.; Saito, T.; Isogai, A.; Koga, H.; Nogi, M. Chemical Modification of Cellulose Nanofibers for the Production of Highly Thermal Resistant and Optically Transparent Nanopaper for Paper Devices. *ACS Appl. Mater. Interfaces* **2015**, *7* (41), 22012–22017.

14. Yagyu, H.; Ifuku, S.; Nogi, M. Acetylation of Optically Transparent Cellulose Nanopaper for High Thermal and Moisture Resistance in a Flexible Device Substrate. *Flex. Print. Electron.* **2017**, *2*, 014003.

15. Song, Y.; Kim, S.; Heller, M. J. An Implantable Transparent Conductive Film with Water Resistance and Ultrabendability for Electronic Devices. *ACS Appl. Mater. Interfaces* **2017**, *9* (48), 42302–42312.

16. Yang, W.; Bian, H.; Jiao, L.; Wu, W.; Deng, Y.; Dai, H. High Wet-Strength, Thermally Stable and Transparent TEMPO-Oxidized Cellulose Nanofibril Film: Via Cross-Linking with Poly-Amide Epichlorohydrin Resin. *RSC Adv.* **2017**, *7* (50), 31567–31573.

17. Kasuga, T.; Isobe, N.; Yagyu, H.; Koga, H.; Nogi, M. Clearly Transparent Nanopaper from Highly Concentrated Cellulose Nanofiber Dispersion Using Dilution and Sonication. *Nanomaterials* **2018**, *8* (2), 104.

18. Isobe, N.; Kasuga, T.; Nogi, M. Clear Transparent Cellulose Nanopaper Prepared from a Concentrated Dispersion by High-Humidity Drying. *RSC Adv.* **2018**, *8* (4), 1833–1837.

19. Kasuga, T.; Yagyu, H.; Uetani, K.; Koga, H.; Nogi, M. “Return to the Soil” Nanopaper Sensor Device for Hyperdense Sensor Networks. *ACS Appl. Mater. Interfaces* **2019**, *11* (46), 43488–43493.

20. Fujisaki, Y.; Koga, H.; Nakajima, Y.; Nakata, M.; Tsuji, H.; Yamamoto, T.; Kurita, T.; Nogi, M.; Shimidzu, N. Transparent Nanopaper-Based Flexible Organic Thin-Film Transistor Array. *Adv. Funct. Mater.* **2014**, *24* (12), 1657–1663.

21. Inui, T.; Koga, H.; Nogi, M.; Komoda, N.; Suganuma, K. A Miniaturized Flexible Antenna Printed on a High Dielectric Constant Nanopaper Composite. *Adv. Mater.* **2015**, *27* (6), 1112–1116.

22. Celano, U.; Nagashima, K.; Koga, H.; Nogi, M.; Zhuge, F.; Meng, G.; He, Y.; De Boeck, J.; Jurczak, M.; Vandervorst, W.; et al. All-Nanocellulose Nonvolatile Resistive Memory. *NPG Asia Mater.* **2016**, *8*, e310.

23. Nagashima, K.; Koga, H.; Celano, U.; Zhuge, F.; Kanai, M.; Rahong, S.; Meng, G.; He, Y.; De Boeck, J.; Jurczak, M.; et al. Cellulose Nanofiber Paper as an Ultra Flexible Nonvolatile Memory. *Sci. Rep.* **2014**, *4*, 5532.

24. Koga, H.; Nogi, M.; Komoda, N.; Nge, T. T.; Sugahara, T.; Suganuma, K. Uniformly Connected Conductive Networks on Cellulose Nanofiber Paper for Transparent Paper Electronics. *NPG Asia Mater.* **2014**, *6*, e93.

25. Saito, T.; Nishiyama, Y.; Putaux, J.-L.; Vignon, M.; Isogai, A. Homogeneous Suspensions of Individualized Microfibrils from TEMPO-Catalyzed Oxidation of Native Cellulose. *Biomacromolecules* **2006**, *7* (6), 1687–1691.

26. Tanaka, R.; Saito, T.; Hänninen, T.; Ono, Y.; Hakalahti, M.; Tammelin, T.; Isogai, A. Viscoelastic Properties of Core-Shell-Structured, Hemicellulose-Rich Nanofibrillated Cellulose in Dispersion and Wet-Film States. *Biomacromolecules* **2016**, *17* (7), 2104–2111.

27. Park, S.; Baker, J. O.; Himmel, M. E.; Parilla, P. A.; Johnson, D. K. Cellulose Crystallinity Index: Measurement Techniques and Their Impact on Interpreting Cellulase Performance. *Biotechnol. Biofuels* **2010**, *3*, 10.

28. Daicho, K.; Kobayashi, K.; Fujisawa, S.; Saito, T. Crystallinity-Independent yet Modification-Dependent True Density of Nanocellulose. *Biomacromolecules* **2020**, *21*, 939–945.

Chapter 3: Li Counterion-Exchanged TEMPO-Oxidized Cellulose Nanofibers as a Copper Electrode Seal for Short-Circuit Failure Inhibition

3.1 Introduction

Due to the increasing demand for miniaturized electronic products, the distances between electronic components, such as printed circuit board traces, have significantly reduced, making electronics more susceptible to failure.[1,2] Electrochemical migration, one of the most severe corrosion issues for electronics, occurs once an electronic device is powered on with water present inside. During electrochemical migration, metallic dendrites form and cause short-circuit failures between nearby components, leading to device collapse and safety hazards.[3–6] To avoid moisture and water ingress and further corrosion failure, devices are usually encapsulated with seals to prevent vapor or moisture from corroding the interior circuitry of electronics. However, electrochemical migration may be initiated at the defects of the seals during practical applications. Additionally, with electronics already playing an essential role in almost every part of our daily life, utilizing biodegradable and renewable materials in electronics is of great importance for the transition to a green society. Accordingly, there is an increasing need to discover a sustainable and more effective approach to the prevention of short-circuit failure for electronics.

Cellulose is well-known as a natural polymer that is mainly found in plants, representing the most abundant bioresource on earth. In recent years, nanocellulose materials, such as cellulose nanofibers, have attracted tremendous interest for use in electronics.[7,8] Although many studies have discussed the working performance and biodegradability of cellulose-based electronic devices,[9–11] the use of cellulose nanofibers to enhance reliability and safety of electronics is still lacks sufficient investigation. Recently, Our group reported a cellulose nanofiber coating on the copper electrode to prevent the short-circuit failure caused by electrochemical migration.[12] Instead of conventional waterproof seals, it can simultaneously form a hydrogel layer to protect copper electrodes. Moreover, cellulose nanofibers with high carboxylate groups, which are known as TEMPO (2,2,6,6-tetramethylpiperidine-1-oxyl radical)-oxidized cellulose nanofibers (TOCNs), were reported to be the most effective at inhibiting short-circuit failure. For example, bare copper electrodes short-circuited within 5 minutes at 3 V with a water droplet. In contrast, TOCN-sealed electrodes did not short-circuit for 24 hours.[12] This study investigated the mechanism of hydrogel formation and demonstrated the potential of using TOCN to prevent short circuits as a new, effective approach. However, a deeper understanding of the underlying

mechanism is needed to optimize its use as electrode seals.

TOCNs are individual nanofibers with homogeneous widths of approximately 3 nm and abundant sodium C6-carboxylate groups on their surfaces. The carboxylate content of TOCNs is controllable from 0.01 mmol/g to ~1.7 mmol/g.[13–15] The carboxylate contents of TOCNs influences their characteristics. For instance, an increase in the carboxylate group content improves the transparency but decreases the heat resistance of TOCN films.[16] The sodium carboxylate groups in TOCNs are counterion-exchangeable, transitioning from protonated to various metal and alkylammonium carboxylate groups.[17] Ion exchange also influences the characteristics of TOCNs, including the density[18], toughness in polymer composites[19], moisture content, oxygen permeability, and flame self-extinction.[20–23] The increase in the carboxylate content during electrochemical migration improves inhibition[12]; however, the effect of counterion exchange has not been reported. In this study, the effect of film properties on prevention of short-circuit failures is focused on. This chapter evaluated the inhibition of electrochemical migration in five types of counterion-exchanged TOCNs. Additionally, an effective TOCN was proposed to prevent short-circuit failures. This chapter evaluated the adhesion and flame resistance of the TOCN films as a copper-electrode sealing layer to realize safe and high-performance electronics using sustainable materials.

3.2 Experimental Section

3.2.1 Preparation of counterion-exchanged TOCNs

A TOCN–water paste (RHEOCRYSTA I-2SX, DKS Co., Ltd., Japan) comprising 2 wt% TOCN and 98 wt% water was used as the starting material. The paste was diluted to 0.3 wt% with distilled water. The resulting TOCNs with sodium carboxylate groups were coded as TOCN–Na.

TOCN–Na was soaked in a dilute HCl solution at pH 2 and room temperature for 2 h.[24] The obtained TOCNs with protonated carboxyl groups were denoted as TOCN–H. Following previous reports, counterion-exchanged TOCNs were prepared from TOCN–H using lithium hydroxide monohydrate, aqueous ammonia solution, and triethylammonium hydroxide,[20–22,25,26] which are denoted as TOCN–Li, TOCN–NH4, and TOCN–TEA, respectively. After the counterion-exchange, these TOCNs were collected by four cycles of centrifugations (12,000 G, 15 min). Their concentration was adjusted to 0.2 wt%, and then they were stirred at 8 000 rpm for 10 min (Homogenizing Mixer Mark II Model 2.5, Primix Corp., Japan). Their zeta potentials were measured using an ELSZ-2000 (Otsuka Electronics Co. Ltd., Japan) with a 0.1 wt% water dispersion.

3.2.2 Analysis

TOCN film preparation

The TOCN films were prepared from five types of TOCN dispersions. Each dispersion (0.2 wt %, 50 g) was evenly distributed into a petri dish and then dried at 55°C and 50% RH in an environmental oven to form the TOCN films (thickness: about 10 μm).

Water-swelling test

For water-swelling test, the TOCN films were soaked into distilled water for 10, 20, 30, 45, and 60 s. The percentage of swollen weight was calculated from the film weights before and after soaking in distilled water (20 mL) at room temperature using the following equation:

$$\text{Swollen ratio}\% = \frac{W_w - W_d}{W_d} \times 100$$

where Ww-weight of the swollen wet TOCN film, Wd-weight of the dried TOCN film.

Redispersion test

For the redispersion test, the TOCN films were crushed into small pieces (1 mm ×1 mm) and soaked in distilled water (kept at the same 0.2wt% concentration with the original dispersion) for 3h, followed by 0.5h stirring. The transmittance of the original and re-dispersed dispersions was measured by a UV-vis-NIR spectrophotometer (UV-3600 Plus, Shimadzu Corp., Kyoto, Japan).

X-ray diffraction (XRD) test

For XRD test, X-ray diffraction patterns were recorded using a Rigaku MiniFlex600 (Tokyo, Japan) with Cu–Kα radiation and a scanning angle (2θ) range of 5–40° at 40 kV voltage and 15 mA current.[27] The crystallinity index of cellulose I was calculated from the (200) reflection (2θ = ca. 22.6°) as previously described. [28,29]

3.2.3 TOCN sealing on interdigitated copper electrodes

Interdigitated copper electrodes were used (IPC-SM-840 pattern B, L/S = 0.318 mm/0.318mm).

The electrodes were ultrasonically cleaned in distilled water for 30 min. After drying, the copper electrode board was masked, except for a 30 mm × 30 mm centered square area. A TOCN layer with a thickness of 5 μm was deposited on the square area of electrodes by dropwise addition of 2 mL TOCN water dispersion on the electrodes, which was followed by drying at 55 °C and 50% RH for 3 h (**Figure 3-1**).

3.2.4 Water-drop test for electrochemical migration

0.5 ml of distilled water (resistivity < 1 μS/cm) was dropped onto the interdigitated copper electrodes with a TOCN sealing. A voltage was applied, and the electrical resistance was measured using a source measurement unit (B2902A, Keysight Technologies, USA). The applied voltage was set at 3 V and the upper current limit was set at 0.1 A (**Figure 3-1**). The measurement time was 6 h. The applied failure criterion was defined as the point at which the interelectrode resistance fell below 20% of the initial resistance.[30]

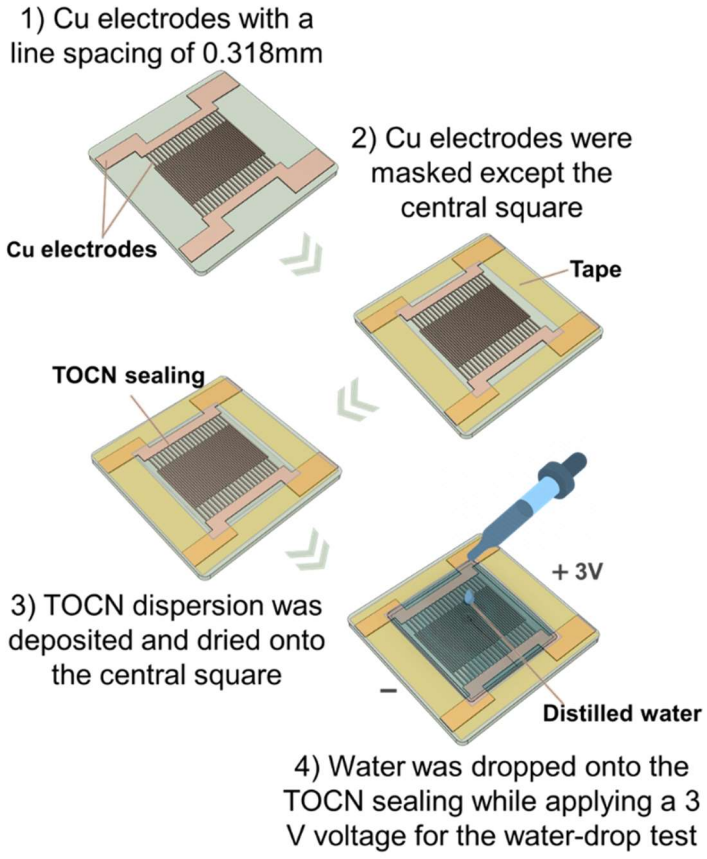

Figure 3-1. Schematic of TOCN sealing on copper electrodes and water-drop test.

3.2.5 Crosshatch-adhesion test

Glass-reinforced epoxy substrate (FR4) and copper substrates were washed with 0.2 wt% NaOH solution and acetone. Their surfaces were modified using plasma under vacuum for 30 s (NMR-Gts, Sakigake-Semiconductor Co., Ltd., Japan). A TOCN layer was deposited on the substrate by dropping water dispersions of 0.5 mL TOCN–Na or TOCN–Li, followed by drying at 55 °C and 50% RH for 3 h. A crosshatch adhesion test was performed to evaluate the adhesion of the TOCN layer on glass-reinforced epoxy or copper substrates. The test was conducted by applying and removing a pressure-sensitive tape (CT-18, Nichiban Co., Ltd., Japan) on the cut areas (30 × 18 mm2) of the film, following the ASTM D3359-B standard.23 The crosshatch patterns (1 × 1 mm2) were formed using a cross-cut guide (CCJ-1, COTEC Corp., Japan). According to this standard, the highest adhesion strength is 5B for no peeling, 4B for less than 5% peeling, 3B for 5-15% peeling, and 0B for more than 65% peeling.

3.2.6 Coefficient of thermal expansion (CTE) test

The CTE values were measured using a thermomechanical analyzer (TMA/SS6100, SII Nanotechnology Inc.). The TOCN–Na and TOCN–Li film specimens (thickness: 40 μm) were 15 mm long and 4 mm wide. The measurements were carried out three times with a heating rate of 5°C/min in a nitrogen atmosphere in tensile mode under a load of 30 mN. The CTE values were determined as the mean values at 20–150 °C in the second run.[31]

3.2.7 Horizontal flammability test

Specimens of 0.03 × 10 × 40 mm3 were prepared from TOCN–Na and TOCN–Li films, and specimens of 0.5 × 10 × 40 mm3 were prepared from epoxy resin. The edges were exposed to a flame for 2 s and was quickly removed.[32]

3.3 Results and Discussion

When a voltage was applied to wet copper electrodes, the copper ions that elute from the anode migrate to the cathode. These migrated ions were then reduced and deposited at the cathode. As the deposited metals grew and reached the anode, the formed dendrites cause short circuits, leading to malfunctions of the electric device. Our previous article proposed that the TOCNs accumulate at the anode because of electrophoresis. Subsequently, the formed cohesive TOCN layers surrounding the

anode inhibited copper ion migration. Moreover, a strong relationship was noted between the short-circuit failure time and carboxylate content of TOCNs.[12] Based on the understanding of hydrogel layer formation around anodes, this study focused on the effect of sealing TOCN layer properties on protection against water-induced short circuit failure.

In situ observations revealed that the sealing TOCN layer first swells into a gel as it absorbs water, and then the negatively charged TOCNs move towards the anode. In this study, the migration inhibition ability of counterion-exchanged TOCNs was considered by focusing on the swelling and redispersing performance of the TOCN seal, rather than the electrophoresis speed of dispersed TOCNs. The zeta potential of the TOCN water dispersion serves as an indicator of the electrophoresis speed of TOCNs under an applied voltage. I used five counterion-exchanged TOCNs with sodium carboxylate groups (TOCN–Na), protonated carboxyl groups (TOCN–H), lithium carboxyl groups (TOCN–Li), ammonium carboxyl groups (TOCN–NH_4), and triethylammonium carboxyl groups (TOCN–TEA). These counterion-exchanged TOCNs were prepared from TOCN-Na with a charge density of 1.6 mmol/g. The Carboxylate groups on the surface of TOCN-Na were first protonated, then the carboxy groups of TOCN-H were neutralized by appropriated metal hydroxides and alkylammonium (equimolar to the carboxyl groups).[24] Therefore, the prepared counterion-exchanged TOCNs have similar zeta potentials ranging from −55 mV to −65 mV (**Figure 3-2**), which indicating similar electrophoresis speed after swelling and dispersion in water.

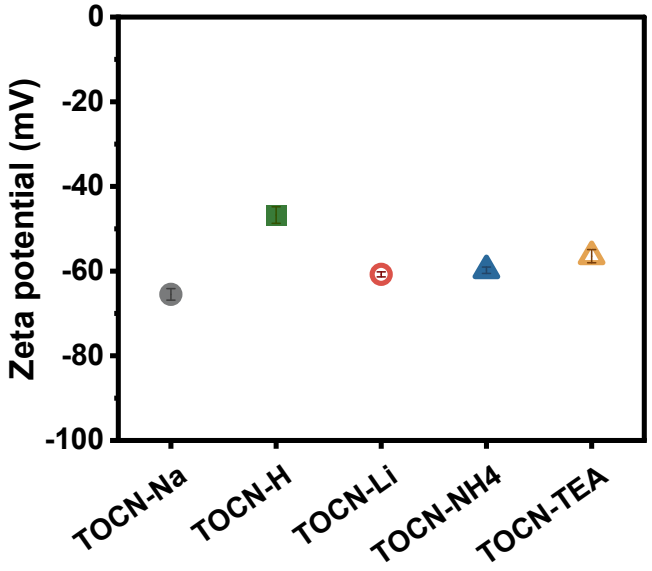

Figure 3-2. Zeta potential of 0.1 wt% water dispersion of TOCN–Na, TOCN–H, TOCN–Li, TOCN–NH_4, and TOCN–TEA.

The hydrophilicity of TOCN films has already been evaluated using various methods, such as the contact angle of a water droplet, water content under saturated humidity, and saturated water uptake.[20–22,24–26] However, hydrophilicity condition in short-circuit failure or migration inhibition are different with these experiments. In particular, short-circuit failures occurred rapidly at <1 min when the electrodes became wet. In this study, I assessed the hydrophilicity by measuring the weight change of the TOCN films before and after soaking in water for 60 s (**Figure 3-3a**). When the TOCN–Na films were immersed in distilled water, they absorbed 34 and 50 wt% water after 10 and 30 s, respectively. The TOCN–Li films exhibited rapid water absorption, reaching 33 wt% and 49 wt% after 10 and 30 seconds, respectively. However, the TOCN–H, TOCN–NH_4, and TOCN–TEA films exhibited considerably lower water-swelling ability at less than 4% after 60 s.

The redispersion test evaluated the redispersibility of counterion-exchanged TOCN films. Dried TOCN films were redispersed in water by soaking and stirring, and the light transmittance at 600 nm of the redispersed TOCN dispersions was measured (**Figure 3-3b and Table 3-1**). TOCN-Na and TOCN-Li exhibited light transmittance values of over 97% compared to the original dispersion, indicating effective redispersion after mechanical disintegration treatment. In contrast, the light transmittance of redispersed TOCN-NH4 and TOCN-TEA recovered only to 40.6% and 61.0%, respectively, compared to the original dispersions. Under the same mechanical treatment, TOCN-NH4 and TOCN-TEA were not sufficiently redispersed, leaving aggregated fibers. TOCN-H demonstrated even worse redispersibility, with only a 30.4% light transmittance recovery compared to its original dispersion. The TOCN-H film was barely redispersed in water, with large pieces observed. Based on X-ray diffraction analysis, the crystallinities of TOCN-Na, TOCN-H, TOCN-Li, TOCN-NH4, and TOCN-TEA were 58.7%, 65.4%, 59.3%, 63.2%, and 54.9%, respectively (**Figure 3-4**). The high crystallinity of TOCN-H and TOCN-NH_4 could explain its low redispersibility, as a high degree of intermolecular hydrogen bonding hinders redispersion in water. For TOCN-TEA, the lower crystallinity index indicated that the intermolecular hydrogen bonds between the hydrophilic surfaces could be inhibited by the bulky TEA ions.[33]

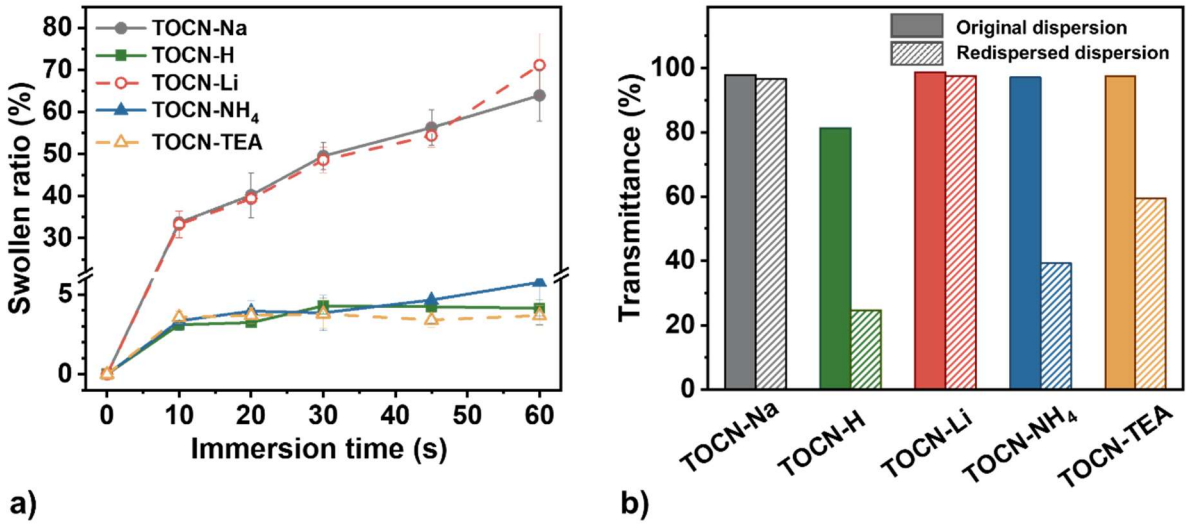

Figure 3-3. a) Swollen ratio of the TOCN films against the immersion time. **b**) Light transmittance at 600 nm of original (solid color) and redispersed (diagonal stripes) TOCN dispersions.

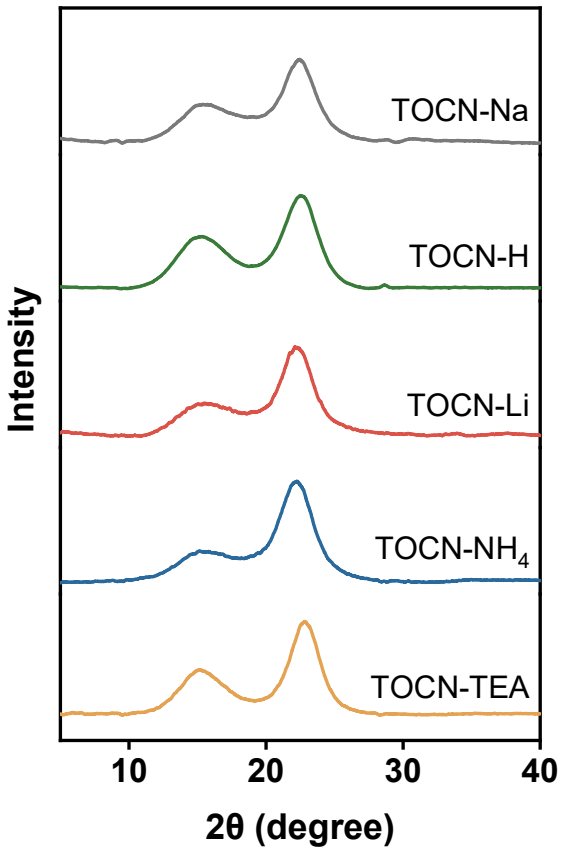

Figure 3-4. XRD spectra of TOCN films.

Table 3-1. Light transmittance (LT) at 600 nm and Transmittance recovery ratio for TOCNs

	LT at 600 nm (%)		Transmittance recovery ratio% ($LT_{Original\ dispersion}/LT_{Redispersed\ dispersion}$)
	Original dispersion	Redispersed dispersion	
TOCN-Na	97.9	96.6	98.7
TOCN-H	81.3	24.7	30.4
TOCN-Li	98.6	97.6	99.0
TOCN-NH_4	97.0.	39.4	40.6
TOCN-TEA	97.4	59.4	61.0

Based on these results, the five TOCNs were categorized into three groups. The first was the metal counterion group, which included TOCN–Na and TOCN–Li; they exhibited high water-swelling ability, high redispersibility, and high electrophoresis speeds. The second was the alkylammonium counterion group, which included TOCN-NH_4 and TOCN-TEA; they exhibited rather low water-swelling ability, low redispersibility, and high electrophoresis speeds. The last was the protonated group of TOCN-H, which had the lowest water-swelling ability and the worst redispersibility with low electrophoresis speed. I then performed a water-drop test for electrochemical migration inhibition using the three groups of TOCN sealings.

Interdigitated copper electrodes with a line and space of 0.318 mm were sealed with a 5-μm-thick layer of TOCN–Na, TOCN–H, TOCN–Li, TOCN–NH_4 or TOCN–TEA. Their electrical resistances were measured for 360 min under an applied voltage of 3 V with 0.5 mL distilled water droplet. The time of failure was recorded when the inter-electrode resistance fell below 20% of the initial resistance (**Figure 3-5 and Figure 3-6**). In the bare copper electrodes without any seal, there was no barrier for copper ion migration, and the short circuit occurred immediately at 0.6 min. Conversely, the effective swelling of the TOCN–Na layer in water prevented copper-ion migration; a short circuit was not observed until 336 min. TOCN–Li showed a similar zeta potential, water-swelling ability, and redispersibility as TOCN–Na, the TOCN–Li-sealed electrodes successfully prevented short circuit for 335 min, which is comparable to that with a TOCN–Na seal. Despite the similar zeta potential of TOCN–NH_4, TOCN–TEA, TOCN–Na, and TOCN–Li, the lower water-swelling ability and rediepseibility of TOCN–NH_4 and TOCN–TEA resulted in a shorter failure time of 7.1 and 17.8 min, respectively. With insufficient swelling and redispersing, less TOCN can be active in water to help prevent short circuits. TOCN–H faces difficulties in preventing copper ion migration. In particular, the

TOCN–H-sealed electrodes exhibited a short-circuit at 1.2 min, because of their low zeta potential, low water-swelling ability, and low redipersibility.

These results align our previous assumption of the sealing layer properties to short-circuit prevention. Combined with our previous understanding of the hydrogel formation around the anode, I can develop a more complete, streamlined mechanism of using TOCN sealings for short-circuit prevention: when the dried TOCN seals became wet, they swelled into a gel, redisperse into water, and then the negatively charged TOCNs moved to the anode, preventing copper ion migration by forming a protective layer. Therefore, the water swelling ability and redispersibility of the TOCN layer are crucial parameters for preventing the short-circuit failure of the electrode sealing material, which could serve as the fundamental standard for selecting TOCN seals for electrodes.

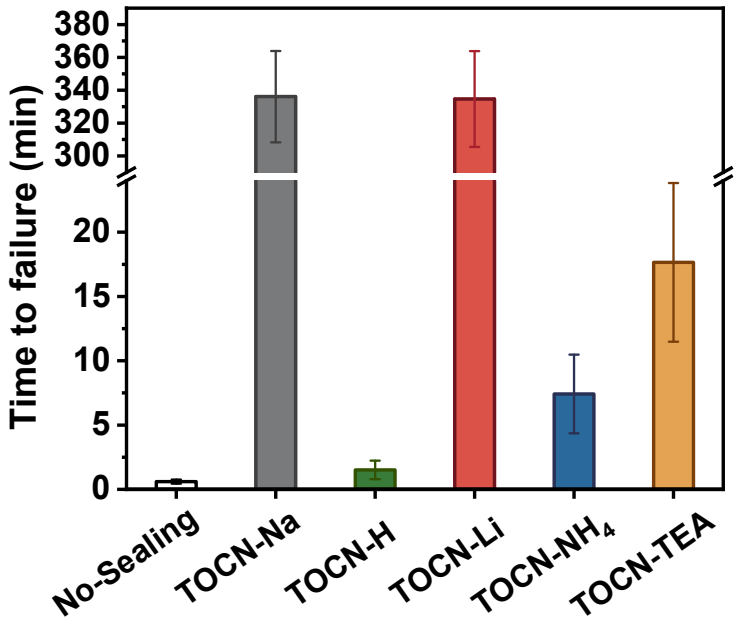

Figure 3-5. Failure time for the TOCN-sealed interdigitated copper electrodes with water droplets.

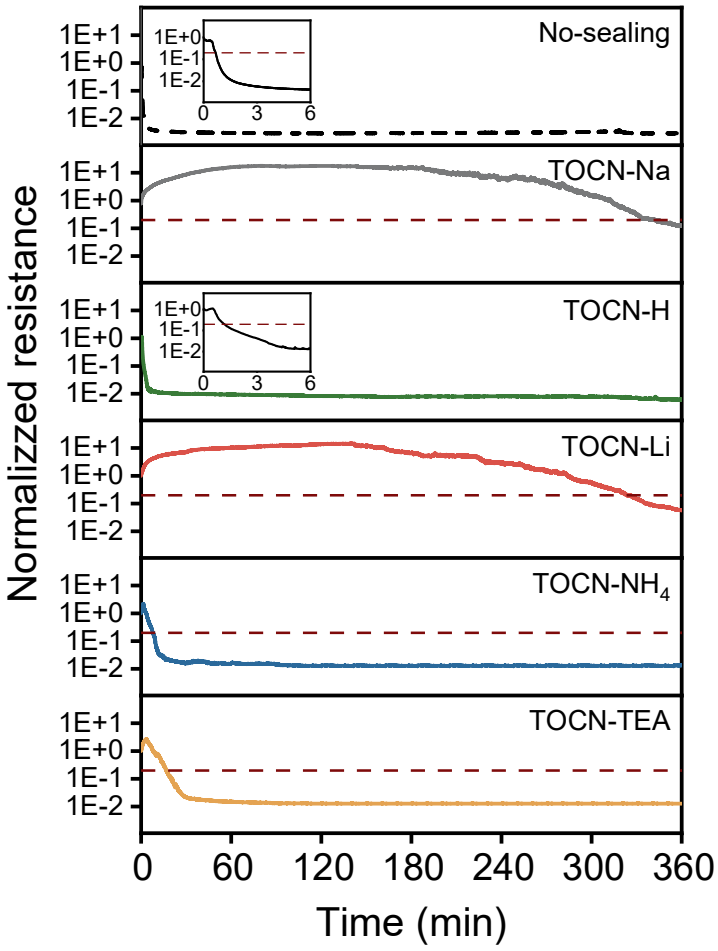

Figure 3-6. Resistance changes referenced to initial resistance during water-drop test. Red dashed line indicates 20% of initial resistance.

These experiments revealed the suitable characteristics of the metal counterion group of TOCN–Na and TOCN–Li layers for preventing short-circuit failures. As sealing materials for device electrodes, TOCN layers are required not only to prevent electrochemical migration, but also ensure good adhesion with the electrodes. The materials undergo thermal expansion or shrinkage depending on ambient temperature changes. In laminated materials with different CTEs for each layer, delamination due to temperature changes is a concern. Therefore, the CTE of the glass-reinforced epoxy substrate (FR4) was designed to be 10–20 ppm/K, which matched that of the copper foil. At 20–140 °C, the CTE of the TOCN–Na and TOCN–Li film were 9.1 and 9.5 ppm/K, respectively (**Figure 3-7**). Therefore, both TOCN layers are of minimal concern for thermal expansion exfoliation from copper electrodes and glass-reinforced epoxy substrates.

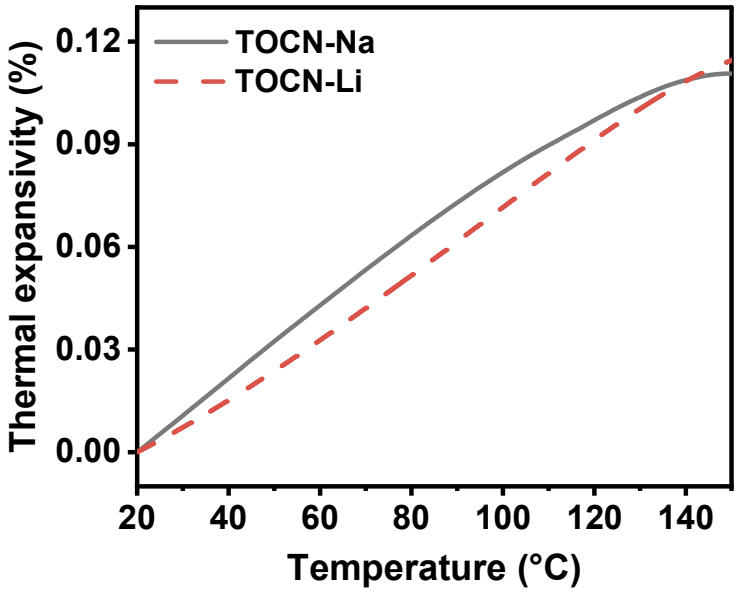

Figure 3-7. CTE of the TOCN films under a nitrogen atmosphere.

Good adhesion is ensured by preventing thermal exfoliation and peeling caused by physical impact. The adhesion strength of the TOCN–Na and TOCN–Li layers was assessed using ASTM D3359-B standard. The peeling from the glass-reinforced epoxy substrates was 3.6% for the TOCN–Na layer and 3.0% for the TOCN–Li layer. Moreover, the peeling from the copper foil substrate was 2.6% for the TOCN–Na layer and 2.2% for the TOCN–Li layer. This result corresponds to the 4B level of adhesion strength, indicating that both TOCN layers adhered well to the glass-reinforced epoxy substrate and conductive copper lines.

Flame retardancy is an essential requirement for electronic device components. In this study, a horizontal flammability test was performed to assess flame retardancy. Epoxy resin is commonly used as a sealing material for device electrodes. However, during the horizontal flammability test, the epoxy film was quickly enveloped in flame upon ignition. Heavy smoke was emitted, and flames often dropped. Ultimately, the epoxy film burned completely after 30 s (**Figure 3-8, upper panel**). Therefore, pure epoxy resin is not suitable as an electrode seal, and flame retardants are commonly added to address this. TOCN–Na is known as a highly fireproof material because of its low heat release capacity, thermally stable char formation.[23] From this experiment, TOCN–Li exhibited rapid flame self-extinction, similar to TOCN–Na. During the horizontal flammability test, both the TOCN–Li and

TOCN–Na films were initially enveloped in flames upon ignition. However, the flames were immediately extinguished when the ignition was changed (**Figure 3-8, middle and lower panels**). Finally, the burning was completely halted within 8 s, leaving over 60% of the film intact.

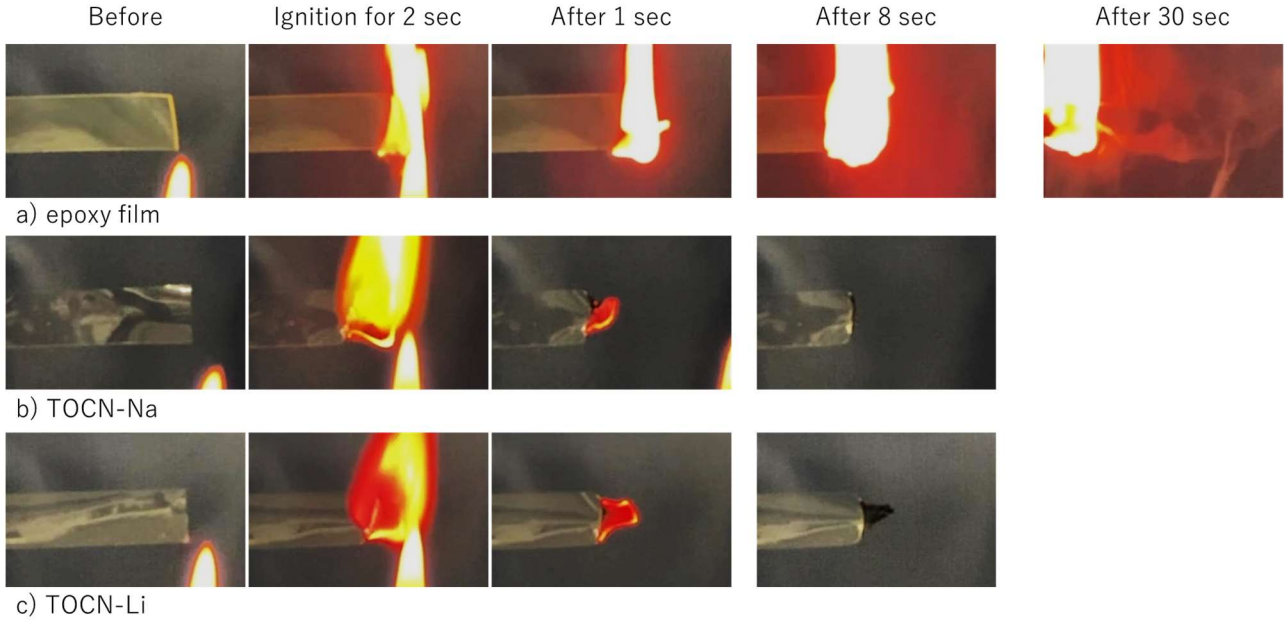

Figure 3-8. Horizontal flammability test. a) Neat epoxy film, b) TOCN–Na film, and c) TOCN–Li film.

3.4 Conclusions

This study investigated the efficacy of various counterion-exchanged TOCN in preventing water-induced short-circuit failures for copper electrodes. The metal counterion group of TOCN–Na and TOCN–Li layers exhibited superior electrophoresis speed, water-swelling ability and redispersibility, resulting in significantly prolonged short-circuit prevention times (336 and 335 minutes, respectively). In contrast, the alkylammonium counterion group of TOCN–NH4 and TOCN–TEA layers showed lower water-swelling and redispersibility, leading to shorter failure times (7.1 and 17.8 minutes, respectively), while TOCN–H displayed the poorest performance with a failure time of just 1.2 minutes. These results validate the critical role of water-swelling ability and redispersibility in enhancing the performance of TOCN layers as protective seals, and expand the mechanism of using TOCN seals for short-circuit protection to include sealing layer behaviors. For practical applications, this study also proved that TOCN–Na and TOCN–Li layers provide excellent thermal compatibility with copper

electrodes and glass-reinforced epoxy substrates, demonstrating minimal concerns for thermal expansion exfoliation and robust adhesion strength. Furthermore, both TOCN–Na and TOCN–Li exhibited exceptional flame retardancy, extinguishing flames rapidly and maintaining structural integrity during flammability tests. These characteristics make TOCN–Na and TOCN–Li promising materials for use in electronic device electrode seals, offering not only protection against short-circuit failures, but also thermal expansion issues and fire hazards. This work provides a foundational understanding of the effect of TOCN sealing layer properties on short-circuit prevention, which can be extended to other cellulose nanofibers and sustainable hydrophilic polymers to improve the reliability of electronics.

3.5 References

1. Noh, B. I.; Jung, S. B. Characteristics of Environmental Factor for Electrochemical Migration on Printed Circuit Board. *J. Mater. Sci. Mater. Electron.* **2008**, *19* (10), 952–956.
2. Medgyes, B.; Illés, B.; Harsányi, G. Electrochemical Migration Behaviour of Cu, Sn, Ag and Sn63/Pb37. *J. Mater. Sci. Mater. Electron.* **2012**, *23* (2), 551–556.
3. Minzari, D.; Grumsen, F. B.; Jellesen, M. S.; Møller, P.; Ambat, R. Electrochemical Migration of Tin in Electronics and Microstructure of the Dendrites. *Corros. Sci.* **2011**, *53* (5), 1659–1669.
4. Zhong, X.; Chen, L.; Medgyes, B.; Zhang, Z.; Gao, S.; Jakab, L. Electrochemical Migration of Sn and Sn Solder Alloys: A Review. *RSC Adv.* **2017**, *7*, 28186–28206.
5. Liao, B.; Wang, H.; Xiao, W.; Cai, Y.; Guo, X. Recent Advances in Method of Suppressing Dendrite Formation of Tin-Based Solder Alloys. *J. Mater. Sci. Mater. Electron.* **2020**, *31*, 13001–13010.
6. Liao, X.; Cao, F.; Zheng, L.; Liu, W.; Chen, A.; Zhang, J.; Cao, C. Corrosion Behaviour of Copper under Chloride-Containing Thin Electrolyte Layer. *Corros. Sci.* **2011**, *53* (10), 3289–3298.
7. Isogai, A. Emerging Nanocellulose Technologies: Recent Developments. *Adv. Mater.* **2021**, *33* (28).
8. Shen, H.; Peng, S.; Luo, Q.; Zhou, J.; He, J. H.; Zhou, G.; Xu, X. Nanopaper Electronics. *Adv. Funct. Mater.* **2023**, *33* (23), 1–36.
9. Dincer, C.; Bruch, R.; Costa-Rama, E.; Fernández-Abedul, M. T.; Merkoçi, A.; Manz, A.; Urban, G. A.; Güder, F. Disposable Sensors in Diagnostics, Food, and Environmental Monitoring. *Adv. Mater.* **2019**, *31* (30).
10. Kasuga, T.; Yagyu, H.; Uetani, K.; Koga, H.; Nogi, M. "Return to the Soil" Nanopaper Sensor Device for Hyperdense Sensor Networks. *ACS Appl. Mater. Interfaces* **2019**, *11* (46), 43488–43493.
11. Kasuga, T.; Mizui, A.; Koga, H.; Nogi, M. Wirelessly Powered Sensing Fertilizer for Precision and Sustainable Agriculture. *Adv. Sustain. Syst.* **2024**, *8* (1), 1–10.
12. Kasuga, T.; Yagyu, H.; Uetani, K.; Koga, H.; Nogi, M. Cellulose Nanofiber Coatings on Cu

Electrodes for Cohesive Protection against Water-Induced Short-Circuit Failures. *ACS Appl. Nano Mater.* **2021**, *4* (4), 3861–3868.

13. Saito, T.; Nishiyama, Y.; Putaux, J. L.; Vignon, M.; Isogai, A. Homogeneous Suspensions of Individualized Microfibrils from TEMPO-Catalyzed Oxidation of Native Cellulose. *Biomacromolecules* **2006**, *7* (6), 1687–1691.

14. Isogai, A.; Saito, T.; Fukuzumi, H. TEMPO-Oxidized Cellulose Nanofibers. *Nanoscale* **2011**, *3* (1), 71–85.

15. Isogai, A.; Hänninen, T.; Fujisawa, S.; Saito, T. Review: Catalytic Oxidation of Cellulose with Nitroxyl Radicals under Aqueous Conditions. *Prog. Polym. Sci.* **2018**, *86*, 122–148.

16. Yagyu, H.; Saito, T.; Isogai, A.; Koga, H.; Nogi, M. Chemical Modification of Cellulose Nanofibers for the Production of Highly Thermal Resistant and Optically Transparent Nanopaper for Paper Devices. *ACS Appl. Mater. Interfaces* **2015**, *7* (39), 22012–22017.

17. Saito, T.; Isogai, A. Ion-Exchange Behavior of Carboxylate Groups in Fibrous Cellulose Oxidized by the TEMPO-Mediated System. *Carbohydr. Polym.* **2005**, *61* (2), 183–190.

18. Daicho, K.; Kobayashi, K.; Fujisawa, S.; Saito, T. Crystallinity-Independent yet Modification-Dependent True Density of Nanocellulose. *Biomacromolecules* **2020**, *21* (2), 939–945.

19. Fujisawa, S.; Saito, T.; Kimura, S.; Iwata, T.; Isogai, A. Surface Engineering of Ultrafine Cellulose Nanofibrils toward Polymer Nanocomposite Materials. *Biomacromolecules* **2013**, *14* (5), 1541–1546.

20. Shimizu, M.; Fukuzumi, H.; Saito, T.; Isogai, A. Preparation and Characterization of TEMPO-Oxidized Cellulose Nanofibrils with Ammonium Carboxylate Groups. *Int. J. Biol. Macromol.* **2013**, *59*, 99–104.

21. Shimizu, M.; Saito, T.; Isogai, A. Bulky Quaternary Alkylammonium Counterions Enhance the Nanodispersibility of 2,2,6,6-Tetramethylpiperidine-1-Oxyl-Oxidized Cellulose in Diverse Solvents. *Biomacromolecules* **2014**, *15* (5), 1904–1909.

22. Benítez, A. J.; Walther, A. Counterion Size and Nature Control Structural and Mechanical Response in Cellulose Nanofibril Nanopapers. *Biomacromolecules* **2017**, *18* (5), 1642–1653.

23. Ishioka, S.; Isobe, N.; Hirano, T.; Matoba, N.; Fujisawa, S.; Saito, T. Fully Wood-Based Transparent Plates with High Strength, Flame Self-Extinction, and Anisotropic Thermal

Conduction. *ACS Sustain. Chem. Eng.* **2023**, *11* (6), 2440–2448.

24. Fujisawa, S.; Okita, Y.; Fukuzumi, H.; Saito, T.; Isogai, A. Preparation and Characterization of TEMPO-Oxidized Cellulose Nanofibril Films with Free Carboxyl Groups. *Carbohydr. Polym.* **2011**, *84* (1), 579–583.

25. Homma, I.; Fukuzumi, H.; Saito, T.; Isogai, A. Effects of Carboxyl-Group Counter-Ions on Biodegradation Behaviors of TEMPO-Oxidized Cellulose Fibers and Nanofibril Films. *Cellulose* **2013**, *20* (5), 2505–2515.

26. Kubo, R.; Saito, T.; Isogai, A. Dual Counterion Systems of Carboxylated Nanocellulose Films with Tunable Mechanical, Hydrophilic, and Gas-Barrier Properties. *Biomacromolecules* **2019**, *20* (4), 1691–1698.

27. Li, C.; Kasuga, T.; Uetani, K.; Koga, H.; Nogi, M. High-Speed Fabrication of Clear Transparent Cellulose Nanopaper by Applying Humidity-Controlled Multi-Stage Drying Method. *Nanomaterials* **2020**, *10* (11).

28. Yagyu, H.; Ifuku, S.; Nogi, M. Acetylation of Optically Transparent Cellulose Nanopaper for High Thermal and Moisture Resistance in a Flexible Device Substrate. *Flex. Print. Electron.* **2017**, *2* (1).

29. Park, S.; Baker, J. O.; Himmel, M. E.; Parilla, P. A.; Johnson, D. K. Cellulose Crystallinity Index: Measurement Techniques and Their Impact on Interpreting Cellulase Performance. *Biofuels* **2010**.

30. Kim, K. S.; Kwon, Y. T.; Choa, Y. H.; Jung, S. B. Electrochemical Migration Behavior of Sn–37Pb and Sn–3.0Ag–0.5Cu Solder Alloys in NaCl Solution. *J. Electron. Mater.* **2007**, *36* (11), 1520–1527.

31. Nogi, M.; Iwamoto, S.; Nakagaito, A. N.; Yano, H. Optically Transparent Nanofiber Paper. *Adv. Mater.* **2009**, *21* (16), 1595–1598.

32. Sakuma, W.; Yamasaki, S.; Fujisawa, S.; Kodama, T.; Shiomi, J.; Kanamori, K.; Saito, T. Mechanically Strong, Scalable, Mesoporous Xerogels of Nanocellulose Featuring Light Permeability, Thermal Insulation, and Flame Self-Extinction. *ACS Nano* **2021**, *15* (1), 1436–1444.

33. Daicho, K.; Kobayashi, K.; Fujisawa, S.; Saito, T. Recovery of the Irreversible Crystallinity of Nanocellulose by Crystallite Fusion: A Strategy for Achieving Efficient Energy Transfers

in Sustainable Biopolymer Skeletons. *Angew. Chemie - Int. Ed.* **2021**, *60* (46), 24630–24636.

Conclusion

In summary, efficient fabrication processes for nanocellulose films were successfully developed using an electrodeposition dehydration method and a new humidity-controlled multi-stage drying method. The electronic application of nanocellulose films as seals was also investigated.

In Chapter 1, electrodeposition was shown to be a promising dehydration method for CNFs. For dilute CNF/water dispersions, electrodeposition dehydration was much more efficient than evaporation. The hierarchical structures of CNFs varied with the applied voltage. Additionally, concentrated CNF hydrogels were reused through neutralization and homogenization, providing new insights into electrodeposition for dehydration and hierarchical control of CNF structures.

In Chapter 2, a multi-stage drying method for high-speed fabrication of clear, transparent nanopaper was reported. Drying experiments revealed that the nanopaper drying process has two periods. Unlike conventional single-stage drying with constant conditions, our method adjusts relative humidity (RH) during these periods. Using a humidity-controllable chamber, this method reduced drying time by 35% while maintaining the same haze level. This multi-stage drying method will help reduce manufacturing time and promote the use of nanopaper-based flexible electronics.

In Chapter 3, the application of nanocellulose films as electronic seals was investigated, focusing on five types of ion-exchanged TOCNs. Key parameters such as water absorption and swelling ability of the TOCN layer are crucial for preventing short-circuit failure. This work lays the foundation for using TOCN seals to prevent short circuits and can be extended to other cellulose nanofibers and sustainable hydrophilic polymers to enhance electronics reliability.

This study paves the way for developing efficient fabrication processes for nanocellulose films and their electronic applications via electrophoretic deposition.

List of Publications

1. Electrodeposition of cellulose nanofibers as an efficient dehydration method

Takaaki Kasuga*,†, Chenyang Li†, Ami Mizui, Shun Ishioka, Hirotaka Koga, Masaya Nogi (†These authors contributed equally to this work)

Carbohydrate Polymers, **2024**, *340*, 122310

DOI: 10.1016/j.carbpol.2024.122310

2. High-Speed Fabrication of Clear Transparent Cellulose Nanopaper by Applying Humidity-Controlled Multi-Stage Drying Method

Chenyang Li, Takaaki Kasuga, Kojiro Uetani, Hirotaka Koga, Masaya Nogi*

Nanomaterials, **2020**, *10*(11), 2194

DOI: 10.3390/nano10112194

3. Li counterion-exchanged TEMPO-oxidized cellulose nanofibers as a copper electrode seal for short-circuit failure inhibition

Chenyang Li, Hitomi Yagyu, Shun Ishioka, Takaaki Kasuga, Hirotaka Koga, Masaya Nogi*

Carbohydrate Polymer Technologies and Applications, **2024**, 100648

DOI: 10.1016/j.carpta.2024.100648

Copyright

Acknowledgements

This study was conducted from 2019 to 2024 at SANKEN and the Department of Applied Chemistry, Graduate School of Engineering, Osaka University.

I would like to express my heartfelt gratitude to Prof. Masaya Nogi, for his unwavering support and guidance in my research and studies since I joined Osaka University. Beyond research, he has also made me understand the many facets of life, greatly strengthening my resilience and forbearance.

I am also deeply grateful to Assoc. Prof. Hirotaka Koga for his invaluable help and thoughtful advice throughout my doctoral studies. His guidance has significantly improved the quality of my work.

My sincere thanks go to Asst. Prof. Takaaki Kasuga, who has been one of my most influential mentors. He has imparted extensive knowledge and practical experimental skills, which have greatly deepened my understanding of cellulosic materials. Our discussions have always been inspiring and thought-provoking.

I would like to thank the Japan Society for the Promotion of Science (JSPS) for their financial support. This study was partially funded by a Grant-in-Aid for Scientific Research from JSPS (Grant Number: JP22KJ2188).

I am also thankful to my lab mates, who have been a significant part of my journey. Luting Zhu has always been a great companion, whether for discussions on research or daily life. Yintong Huang has been a constant source of support, offering both company and help when needed. Shuyun Li has provided me with immense emotional encouragement. I am also grateful to other members of the Nogi lab, with whom I have worked closely over the past five years.

I extend my thanks to my friends, who have always been there for me. Over time, I have come to deeply appreciate the tremendous support friends can offer, and I have benefited greatly from it.

Special thanks also go to my cat, Mesa. Raising her and ensuring her health has been one of the most meaningful accomplishments of my doctoral years.

Lastly, I would like to express my appreciation to my family, especially my parents. Their selfless emotional and material support has been a pillar of strength, reinforcing my determination to pursue my ambitions in life. I would like to express my deepest appreciation to my grandpa, who was my first and forever teacher. Although he did not live to see me graduate, the way he raised me has always stayed with me, and not a single day goes by without me missing him.

Stripping away all the gratitude, I can't say that my life as a PhD student was particularly joyful—it was especially challenging in the last year and half. I lost much but gained little. During this time, I developed the habit of taking moments to look at the sky and the leaves. Gradually, as I observed them, I came to accept reality. The reality is that I made my choices, worked hard, and made many mistakes. After accepting this reality, I've slowly learned to embrace my less-than-perfect self and stopped undervaluing the passion and sincerity I poured into these years.

I've messed up many things, and I'm capable of messing up many more. I will probably continue to make mistakes in the future.

By the end of my PhD, I felt like I had gone so long without absorbing new knowledge that I almost forgot I was still a student. But perhaps being a student is something that never truly ends in life.

To close with a cliché, I still want to say it:

人生海海，山山而川，不过尔尔。要尽兴，开怀。

Chenyang Li

June 2024

And December 2024